High-intensity third-harmonic generation

Paul S. Banks,* Michael D. Feit, and Michael D. Perry*

Laser Program, Lawrence Livermore National Laboratory, P.O. Box 808, L-477, Livermore, California 94550

Received February 19, 2001

The azimuthal dependence of third-order and cascaded second-order nonlinear coupling are used to measure the relative contributions of each to direct third-harmonic generation in β-barium borate. This enabled the measurement of the values of $\chi_{10}^{(3)}$, $\chi_{11}^{(3)}$, and $\chi_{16}^{(3)}$ relative to the known $\chi_{ij}^{(2)}$. Finally, conversion efficiencies to 3ω of up to 6% from a single crystal were achieved with a femtosecond chirped-pulse-amplification laser with 200 GW/cm^2 in collimated beams. © 2002 Optical Society of America

OCIS codes: 190.0190, 190.2620, 190.7110, 190.4400, 190.7220.

1. INTRODUCTION

Almost from the demonstration of lasers, nonlinear interactions have been used to convert the frequency of laser light to the third harmonic. However, efforts in solid media to use higher-order processes for this have been limited because of low conversion efficiencies. Research has also been done by use of focusing geometries in liquids and gases,[1–4] but for efficient third-harmonic generation (THG) it is usually understood that this refers to the two-step process of first phase-matched second-harmonic generation (SHG) followed by phase-matched sum-frequency generation (SFG) of the generated 2ω light with the remaining fundamental in a separate nonlinear crystal. In solids, this has been because the nonlinear coupling for higher-order processes has been too low for efficient conversion at intensities below the threshold for material damage (typically less than a few GW/cm^2 for nanosecond lasers). However, it is known that the intensity damage threshold for transparent dielectrics increases roughly as the inverse of the square root of the pulse length down to pulse lengths of 1–10 ps.[5] This means that for a 1-ps pulse the damage threshold would be several hundred GW/cm^2. For shorter pulses the threshold increases even more rapidly with decreasing pulse length.

The recent advances in the technique known as chirped-pulse amplification[6,7] has resulted in the proliferation of tabletop lasers capable of producing beams with peak powers of one terawatt and beyond. This technology, combined with the increased damage threshold, enables experiments at high intensities (>100 GW/cm^2) in collimated beams in solid-state material without the risk of damage. This opens for study an entirely new realm of nonlinear interactions in solid materials. In particular, it allows the possibility of efficiently generating the third harmonic by use of the third-order susceptibility in a single nonlinear crystal.

The use of the third-order susceptibility also means that the optimal material may be different than those currently used for frequency conversion. Values for the individual tensor elements of the third-order susceptibility are relatively unknown. There are also often large discrepancies among the values that are reported in the literature, which makes material choice difficult. Some possible choices can be eliminated because our objective is ultimately to generate the third harmonic of near-infrared solid-state lasers. Thus materials of interest need to be transparent into the UV, phase matchable at these wavelengths, and available in high quality in relatively large sizes.

A few recent studies of single-crystal THG in solid materials have been done, particularly in beta-barium borate, β-BaB_2O_4 (BBO),[8,9] with low-energy, mode-locked pulses with pulse lengths from 5 to 45 ps. Qiu and Penzkofer[8] saw up to 1% conversion in phase-matched THG with 50 GW/cm^2 in a focused-beam geometry. They indicated (as well as others[10–14]) that non-phase-matched, cascaded second-order processes can contribute to THG in addition to the phase-matched contribution due to the third-order susceptibility. However, the experimental uncertainties were too large to ascertain the extent of the second-order contribution.

In this paper we have chosen to further explore the use of noncentrosymmetric crystals for efficient single-crystal THG. In particular, we distinguish between the second- and third-order coupling in BBO by using the different azimuthal dependences of the effective coupling terms. We separate the second- and third-order contributions and show that the largest contribution to THG is from the non-phase-matched second-order processes. This also enabled us to determine the values for several of the tensor elements of $\chi^{(3)}$ relative to the known elements of $\chi^{(2)}$. In addition, we numerically solved the coupled system of equations describing all possible interactions and investigated the maximum efficiency achievable at intensities up to 1 TW/cm^2. Finally, we measured the conversion efficiencies to the third harmonic for input irradiances up to 200 GW/cm^2 in a Gaussian beam in BBO, deuterated organic salt L-arginine phosphate (d-LAP) and potassium dideuterium phosphate (KD*P) with efficiencies reaching 6% in BBO.

2. COUPLED-WAVE EQUATIONS

In this paper we focus on third-harmonic generation in a single crystal, birefringently phase matched for the pro-

cess $\omega + \omega + \omega \rightarrow 3\omega$. For interactions involving such high irradiances, it is necessary to account for other third-order interactions in the model, including phase modulation. As mentioned above, all possible non-phase-matched second-order interactions that can contribute to the third-harmonic wave must also be accounted for.

For THG there are three possible permutations of the polarization of the three input waves, which we will specify as (following formalism of Webb *et al.*[15])

Type I slow+slow+slow → fast,

Type II slow+slow+fast → fast,

Type III slow+fast+fast → fast,

where the order on the left side of the arrow is unimportant (the three waves are of the same wavelength).

If only third-harmonic generation is phase matched, the significant waves are normally the fundamental (with both possible polarizations) and the third harmonic. The second-harmonic waves (both polarizations) are also significant and need to be included. To simplify the notation in the following, these waves will be denoted with subscripts defined in the following way:

(1) 1ω (slow polarization),

(2) 1ω (fast polarization),

(3) 2ω (slow polarization),

(4) 2ω (fast polarization),

(5) 3ω (fast polarization).

This means that $\omega_1 = \omega_2 = \omega_0$, $\omega_3 = \omega_4 = 2\omega_0$, and $\omega_5 = 3\omega_0$. The set of wave equations governing the total interaction under the slowly varying envelope approximation will then be (including all phase-matched third-order processes)

$$\begin{aligned}\frac{\partial A_1}{\partial z} = & -\beta_{11}\frac{\partial A_1}{\partial t} - \frac{i}{2}\beta_{21}\frac{\partial^2 A_1}{\partial t^2} + \frac{i}{2k_1}\nabla_\perp^2 A_1 \\ & + \frac{i\omega_1}{n_1 c}\left(\frac{3C_1^{\mathrm{SPM}}}{2}|A_1|^2 A_1 + 3C_1^{\mathrm{XPM}}|A_5|^2 A_1\right. \\ & \left. + 3C_2^{\mathrm{XPM}}|A_2|^2 A_1\right) + \frac{i\omega_1}{n_1 c}\Big[d_1 A_3 A_1^* \exp(i\Delta k_1 z) \\ & + d_3 A_4 A_1^* \exp(i\Delta k_3 z) + d_2 A_3 A_2^* \exp(i\Delta k_2 z) \\ & + d_4 A_4 A_2^* \exp(i\Delta k_4 z) + d_5 A_5 A_4^* \exp(i\Delta k_5 z) \\ & + d_7 A_5 A_3^* \exp(i\Delta k_7 z) \\ & + 3C_1 A_5 A_2^* A_1^* \exp(i\Delta k_{11} z) \\ & + \frac{3C_2}{2}A_5 A_1^{*2}\exp(i\Delta k_{12} z) \\ & + \frac{3C_3}{2}A_5 A_2^{*2}\exp(i\Delta k_{13} z)\Big], \end{aligned} \tag{1}$$

$$\begin{aligned}\frac{\partial A_2}{\partial z} = & -\beta_{12}\frac{\partial A_2}{\partial t} - \frac{i}{2}\beta_{22}\frac{\partial^2 A_2}{\partial t^2} + \frac{i}{2k_2}\nabla_\perp^2 A_2 \\ & + \frac{i\omega_2}{n_2 c}\left(\frac{3C_2^{\mathrm{SPM}}}{2}|A_2|^2 A_2 + 3C_3^{\mathrm{XPM}}|A_5|^2 A_2\right. \\ & \left. + 3C_4^{\mathrm{XPM}}|A_1|^2 A_2\right) + \frac{i\omega_2}{n_2 c}\Big[d_2 A_3 A_1^* \exp(i\Delta k_2 z) \\ & + d_4 A_4 A_1^* \exp(i\Delta k_4 z) + d_6 A_5 A_4^* \exp(i\Delta k_6 z) \\ & + d_8 A_5 A_3^* \exp(i\Delta k_8 z) + d_9 A_3 A_2^* \exp(i\Delta k_9 z) \\ & + d_{10} A_4 A_2^* \exp(i\Delta k_{10} z) \\ & + \frac{3C_1}{2}A_5 A_1^{*2}\exp(i\Delta k_{11} z) \\ & + 3C_3 A_5 A_1^* A_2^* \exp(i\Delta k_{13} z)\Big], \end{aligned} \tag{2}$$

$$\begin{aligned}\frac{\partial A_3}{\partial z} = & -\beta_{13}\frac{\partial A_3}{\partial t} - \frac{i}{2}\beta_{23}\frac{\partial^2}{A_3}\partial t^2 + \frac{i}{2k_3}\nabla_\perp^2 A_3 \\ & + \frac{i\omega_3}{n_3 c}\left(\frac{3C_3^{\mathrm{SPM}}}{2}|A_3|^2 A_3 + 3C_5^{\mathrm{XPM}}|A_5|^2 A_3\right. \\ & \left. + 3C_6^{\mathrm{XPM}}|A_2|^2 A_3 + 3C_7^{\mathrm{XPM}}|A_1|^2 A_3\right) \\ & + \frac{i\omega_3}{n_3 c}\Big[\frac{d_1}{2}A_1^2\exp(-i\Delta k_1 z) \\ & + d_2 A_2 A_1 \exp(-i\Delta k_2 z) + \frac{d_9}{2}A_2^2\exp(-i\Delta k_9 z) \\ & + d_7 A_5 A_1^* \exp(i\Delta k_7 z) + d_8 A_5 A_2^* \exp(i\Delta k_8 z)\Big], \end{aligned} \tag{3}$$

$$\begin{aligned}\frac{\partial A_4}{\partial z} = & -\beta_{14}\frac{\partial A_4}{\partial t} - \frac{i}{2}\beta_{24}\frac{\partial^2 A_4}{\partial t^2} + \frac{i}{2k_4}\nabla_\perp^2 A_4 \\ & + \frac{i\omega_4}{n_4 c}\left(\frac{3C_3^{\mathrm{SPM}}}{2}|A_4|^2 A_4 + 3C_8^{\mathrm{XPM}}|A_5|^2 A_4\right. \\ & \left. + 3C_9^{\mathrm{XPM}}|A_2|^2 A_4 + 3C_{10}^{\mathrm{XPM}}|A_1|^2 A_4\right) \\ & + \frac{i\omega_4}{n_4 c}\Big[\frac{d_3}{2}A_1^2\exp(-i\Delta k_3 z) \\ & + d_4 A_2 A_1 \exp(-i\Delta k_4 z) + \frac{d_{10}}{2}A_2^2\exp(-i\Delta k_{10} z) \\ & + d_5 A_5 A_1^* \exp(i\Delta k_5 z) + d_6 A_5 A_2^* \exp(i\Delta k_6 z)\Big], \end{aligned} \tag{4}$$

$$\frac{\partial A_5}{\partial z} = -\beta_{15}\frac{\partial A_5}{\partial t} - \frac{i}{2}\beta_{25}\frac{\partial^2 A_5}{\partial t^2} + \frac{i}{2k_5}\nabla_\perp^2 A_5 + \frac{i\omega_5}{n_5 c}\left(\frac{3C_5^{\mathrm{SPM}}}{2}|A_5|^2 A_5 + 3C_{11}^{\mathrm{XPM}}|A_2|^2 A_5 + 3C_{12}^{\mathrm{XPM}}|A_1|^2 A_5\right) + \frac{i\omega_5}{n_5 c}\left[d_5 A_4 A_1 \exp(-i\Delta k_5 z) + d_6 A_4 A_2 \exp(-i\Delta k_6 z) + d_7 A_3 A_1 \exp(-i\Delta k_7 z) + d_8 A_3 A_2 \exp(-i\Delta k_8 z) + \frac{3C_1}{2}A_1^2 A_2 \exp(-i\Delta k_{11} z) + \frac{C_2}{2}A_1^3 \exp(-i\Delta k_{12} z) + \frac{3C_3}{2}A_1 A_2^2 \exp(-i\Delta k_{13} z)\right]. \quad (5)$$

In these equations, A_j represent the slowly varying portion of the complex electric field, $E_j = \{A_j \exp[i(kz - \omega t)] + A_j^* \exp[-i(kz - \omega t)]\}/2$, $\beta_{1j} = \partial k(\omega)/\partial\omega|_{\omega_j}$, and $\beta_{2j} = \partial^2 k(\omega)/\partial\omega^2|_{\omega_j}$.

The terms Δk_j are defined as

$$\begin{aligned}
\Delta k_1 &= k_3 - 2k_1, & \Delta k_2 &= k_3 - k_1 - k_2,\\
\Delta k_3 &= k_4 - 2k_1, & \Delta k_4 &= k_4 - k_1 - k_2,\\
\Delta k_5 &= k_5 - k_4 - k_1, & \Delta k_6 &= k_5 - k_4 - k_2,\\
\Delta k_7 &= k_5 - k_3 - k_1, & \Delta k_8 &= k_5 - k_3 - k_2,\\
\Delta k_9 &= k_3 - 2k_2, & \Delta k_{10} &= k_4 - 2k_2,\\
\Delta k_{11} &= k_5 - 2k_1 - k_2, & \Delta k_{12} &= k_5 - 3k_1,\\
\Delta k_{13} &= k_5 - k_1 - 2k_2. &&
\end{aligned}$$

The coefficients d_j and C_j are the effective nonlinear coupling coefficients, defined in terms of the nonlinear susceptibilities as

$$d_j = \hat{\mathbf{e}}_1 \cdot \boldsymbol{\chi}^{(2)} : \hat{\mathbf{e}}_2\hat{\mathbf{e}}_3/2,\ j = 1\text{–}10, \quad (6)$$

$$C_{j-10} = \hat{\mathbf{e}}_1 \cdot \boldsymbol{\chi}^{(3)} : \hat{\mathbf{e}}_2\hat{\mathbf{e}}_3\hat{\mathbf{e}}_4/4,\ j = 11\text{–}13, \quad (7)$$

where $\hat{\mathbf{e}}_k$ represents a unit vector in the polarization direction of the kth wave in the order given for Δk_j above. The factors of 1/2 and 3 appearing in Eqs. (1)–(5) are due to the degeneracy in polarization and wavelength that appears in some of the terms (see, for example, p. 26 of Ref. 16). In Eqs. (1), (2), and (5), the contribution due to cross-phase modulation by the second-harmonic wave has been neglected, since this wave will never reach appreciable intensities. All interactions are assumed to be collinear, i.e., all waves propagate parallel to the z axis in lab frame.

3. CASCADED THIRD-HARMONIC GENERATION

It is instructive to simplify Eqs. (1)–(5) greatly in order to observe the effect of the second-harmonic term. Ordinarily, such terms would be neglected because they are not phase matched. However, as has been shown previously,[8,10,11,17–19] because the third-harmonic and fundamental waves are phase matched allows for the possibility of conversion to the third harmonic even with no third-order coupling ($C_j = 0$), as illustrated in Fig. 1.

For low conversion the fundamental waves can be assumed to be constant (no pump depletion, i.e., $\partial A_1/\partial z = \partial A_2/\partial z \simeq 0$), and, to good approximation, the individual interactions can be assumed to be independent of each other. For illustration, let us examine type I phase matching and consider the interaction $ss \rightarrow s + ss \rightarrow f$. Finally, let us neglect longitudinal and transverse spatial dependence of the pulse as well as self- ($C_j^{\mathrm{SPM}} = 0$) and cross-phase modulation ($C_j^{\mathrm{XPM}} = 0$) for simplicity. Eqs. (1)–(5) then reduce to

$$\frac{\partial A_1}{\partial z} = \frac{i\omega_1}{n_1 c}\left[d_1 A_3 A_1^* \exp(i\Delta k_1 z) + d_7 A_5 A_3^* \exp(i\Delta k_7 z) + \frac{3C_2}{2}A_5 A_1^{*2} \exp(i\Delta k_{12} z)\right] \simeq 0, \quad (8)$$

$$\frac{\partial A_3}{\partial z} = \frac{i\omega_3}{n_3 c}\left[\frac{d_1}{2}A_1^2 \exp(-i\Delta k_1 z) + d_7 A_5 A_1^* \exp(i\Delta k_7 z)\right], \quad (9)$$

$$\frac{\partial A_5}{\partial z} = \frac{i\omega_5}{n_5 c}\left[d_7 A_3 A_1 \exp(-i\Delta k_7 z) + \frac{C_2}{2}A_1^3 \exp(-i\Delta k_{12} z)\right]. \quad (10)$$

If the third-order interaction is neglected for the moment as a further simplification ($C_2 = 0$) and Δk_{12} is set to 0 (i.e., perfect phase matching for THG), these equations can be solved analytically. By making a substitution of $f(z) = A_3 \exp(-i\Delta k_7 z)$ in Eqs. (9) and (10) and then differentiating Eq. (9) and substituting Eqs. (10) and (9) into the result, we obtain a second-order ordinary differential equation with constant coefficients. The solution to this is straightforward, and the final solutions are

$$A_3(z) = \frac{i\omega_3}{2n_3 c\zeta}d_1 A_1^2 \exp(i\Delta k_7 z/2)\sin\zeta z, \quad (11)$$

$$A_5(z) = \frac{d_1 A_1^2}{2d_7 A_1^*}\left[\exp(-i\Delta k_7 z/2) \times \left(\cos\zeta z + \frac{\Delta k_7}{2\zeta}\sin\zeta z\right) - 1\right], \quad (12)$$

with

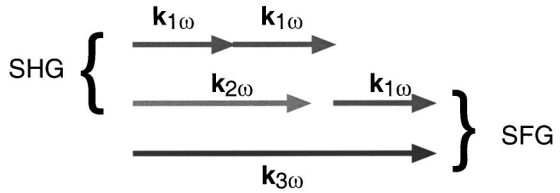

Fig. 1. Illustration of processes involved in third-harmonic generation by cascaded second-order processes. The first process is SHG ($\omega + \omega \rightarrow 2\omega$, indicated by the left brace) followed by sum-frequency generation (SFG, $2\omega + \omega \rightarrow 3\omega$, indicated by the right brace). The space between $\mathbf{k}_{2\omega}$ and $\mathbf{k}_{1\omega}$ on the second line indicates a possible phase mismatch for SHG and SFG processes.

$$\zeta^2 = \frac{\omega_5\omega_3}{n_5 n_3 c^2} d_7^2 |A_1|^2 + \left(\frac{\Delta k_7}{2}\right)^2. \tag{13}$$

When converted to intensities ($I = c\epsilon_0 n|A|^2/2$), these become

$$I_3(z) = \left(\frac{\omega_3}{n_1 c\zeta}\right)^2 \frac{d_1 I_1^2}{\epsilon_0 c n_3} \sin^2 \zeta z, \tag{14}$$

$$I_5(z) = \frac{d_1^2 n_5 I_1}{4 n_1 d_7^2}\left(1 + \cos^2 \zeta z + \frac{\Delta k_7^2}{4\zeta^2}\sin^2 \zeta z - 2\cos \zeta z \cos\frac{\Delta k_7 z}{2} - \frac{\Delta k_7}{\zeta}\sin \zeta z \sin\frac{\Delta k_7 z}{2}\right). \tag{15}$$

Although Eq. (15) appears to have only a linear dependence on the input fundamental intensity I_1, a further approximation can be made for most circumstances where the phase mismatch for SFG is large, i.e., $\eta \ll \Delta k_7$, where

$$\eta = \frac{\omega_5\omega_3}{n_5 n_3 c^2}\frac{d_7^2}{\Delta k_7}|A_1|^2. \tag{16}$$

The approximation $\zeta \simeq \eta + \Delta k_7/2$ can then be made, and Eq. (15) takes on the following approximate form (again, no third-order coupling):

$$I_5(z) = \left(\frac{\omega_3}{n_3 c \Delta k_7}\right)^2 \frac{\omega_5^2 (d_1 d_7)^2}{n_5 n_1^3 \epsilon_0^2 c^4} I_1^3 z^2. \tag{17}$$

This compares with the standard solution for THG involving only the third-order nonlinear susceptibility of [setting $d_j = 0$ in Eqs. (9) and (10)]

$$I_5(z) = \frac{\omega_5^2 C_2^2}{n_5 n_1^3 \epsilon_0^2 c^4} I_1^3 z^2. \tag{18}$$

It is clear that these two solutions have the same form if one defines an effective nonlinear coefficient C_{eff} for the cascaded second-order process as

$$C_{\text{eff}} = \frac{\omega_3}{n_3 c \Delta k_7} d_1 d_7. \tag{19}$$

With the first term in the parentheses in Eq. (17) equal to roughly 15–30 for typical values of ω, n, and Δk and d_j being $\sim 10^{-12}$ m/V, $C_{\text{eff}} \cong 10^{-23} - 10^{-22}$ m^2/V^2. This is in the same range as is expected for the values of C due solely to the third-order susceptibility. In fact, Bloembergen[10] states that the contributions from these two processes should be of the same order of magnitude.

A. Effective Nonlinear Coupling

It is therefore necessary to account for all possible second-order interactions for each THG phase-matching type, including ones not typically phase matchable (Table 1). Of course, all interactions can take place for any phase-matching configuration. However, for each phase-matching configuration, the overall phase-matching requirements, as well as which waves exist at input, limit contributions to efficient THG to only those interactions shown in Table 1.

Table 1. Possible Interactions for THG[a]

	Interaction		
Phase-Matching Type	SHG	SFG	THG
Type I			
	ss → s	ss → f	
	ss → f	sf → f	
			sss → f
Type II			
	ss → s	fs → f	
	sf → s	ss → f	
	ss → f	ff → f	
	sf → f	sf → f	
			ssf → f
Type III			
	sf → s	fs → f	
	ff → s	ss → f	
	sf → f	ff → f	
	ff → f	sf → f	
			sff → f

[a] The polarization directions *f*/*s* are given in order of longest wavelength to shortest.

Table 2. Effective Nonlinear Coefficient for Second-Order Interactions, Neglecting Dispersion (sss Interactions)

Crystal Class	d_{eff}
3	$-d_{11}\sin 3\phi - d_{22}\cos 3\phi$
$3m$	$-d_{22}\cos 3\phi$
$\bar{6}$	$-d_{11}\sin 3\phi - d_{22}\cos 3\phi$
6 and 4	0
$6mm$ and $4mm$	0
622 and 422	0
$\bar{6}m2$	$-d_{22}\cos 3\phi$
$\bar{4}$	0
32	$-d_{11}\sin 3\phi$
$\bar{4}2m$, $\bar{4}3m$, and 23	0

Table 3. Effective Nonlinear Coefficient for Second-Order Interactions, Neglecting Dispersion (ssf Interactions)

Crystal Class	d_{eff}
3	$\cos\theta_m(d_{11}\cos 3\phi - d_{22}\sin 3\phi) + d_{31}\sin\theta_m$
$3m$	$-d_{22}\cos\theta_m \sin 3\phi + d_{31}\sin\theta_m$
$\bar{6}$	$\cos\theta_m(d_{11}\cos 3\phi - d_{22}\sin 3\phi)$
6 and 4	$d_{31}\sin\theta_m$
$6mm$ and $4mm$	$d_{31}\sin\theta_m$
622 and 422	0
$\bar{6}m2$	$-d_{22}\cos\theta_m \sin 3\phi$
$\bar{4}$	$-\sin\theta_m(d_{31}\cos 2\phi + d_{36}\sin 2\phi)$
32	$d_{11}\sin\theta_m \cos 3\phi$
$\bar{4}2m$, $\bar{4}3m$, and 23	$-d_{36}\sin\theta_m \sin 2\phi$

Table 4. Effective Nonlinear Coefficient for Second-Order Interactions, Neglecting Dispersion (sff Interactions)

Crystal Class	d_{eff}
3	$\cos^2\theta_m(d_{11}\sin 3\phi + d_{22}\cos 3\phi)$
$3m$	$d_{22}\cos^2\theta_m\cos 3\phi$
$\bar{6}$	$\cos^2\theta_m(d_{11}\sin 3\phi + d_{22}\cos 3\phi)$
6 and 4	0
$6mm$ and $4mm$	0
622 and 422	0
$\bar{6}m2$	$d_{22}\cos^2\theta_m\cos 3\phi$
$\bar{4}$	$\sin 2\theta_m(d_{36}\cos 2\phi - d_{31}\sin 2\phi)$
32	$d_{11}\cos^2\theta_m\sin 3\phi$
$\bar{4}2m$, $\bar{4}3m$, and 23	$\sin 2\theta_m d_{36}\cos 2\phi$

Table 5. Effective Nonlinear Coefficient for Second-Order Interactions, Neglecting Dispersion (fff Interactions)

Crystal Class	d_{eff}
3	$\cos^3\theta_m(-d_{11}\cos 3\phi + d_{22}\sin 3\phi) + 3d_{31}\sin\theta_m\cos^2\theta_m + d_{33}\sin^3\theta_m$
$3m$	$d_{22}\cos^3\theta_m\sin 3\phi + 3d_{31}\sin\theta_m\cos^2\theta_m + d_{33}\sin^3\theta_m$
$\bar{6}$	$\cos^3\theta_m(-d_{11}\cos 3\phi + d_{22}\sin 3\phi)$
6 and 4	$3d_{31}\sin\theta_m\cos^2\theta_m + d_{33}\sin^3\theta_m$
$6mm$ and $4mm$	$3d_{31}\sin\theta_m\cos^2\theta_m + d_{33}\sin^3\theta_m$
622 and 422	0
$\bar{6}m2$	$d_{22}\cos^3\theta_m\sin 3\phi$
$\bar{4}$	$3\sin\theta_m\cos^2\theta_m(d_{36}\sin 2\phi + d_{31}\cos 2\phi)$
32	$-d_{11}\cos^3\theta_m\cos 3\phi$
$\bar{4}2m$, $\bar{4}3m$, and 23	$3d_{36}\sin\theta_m\cos^2\theta_m\sin 2\phi$

Table 6. Effective Nonlinear Coefficient for Third-Order Interactions, Neglecting Dispersion (ssss Interactions)

Crystal Class	C_{eff}
Trigonal (3 and $\bar{3}$)	C_{11}
Trigonal ($3m$, $\bar{3}m$, and 32)	C_{11}
Hexagonal (6, $\bar{6}$, $6/m$, 622, $6mm$, $6/mmm$, and $\bar{6}m2$)	C_{11}
Tetragonal (4, $\bar{4}$, and $4/m$)	$\frac{1}{4}[C_{11}(3+\cos 4\phi) + 6C_{18}\sin^2 2\phi] + C_{21}\sin 4\phi$
Tetragonal ($\bar{4}2m$, 422, $4mm$, and $4/mmm$)	$\frac{1}{4}[C_{11}(3+\cos 4\phi) + 6C_{18}\sin^2 2\phi]$
Cubic (23, $m3$, 432, $\bar{4}3m$, and $m3m$)	$\frac{1}{4}[C_{11}(3+\cos 4\phi) + 6C_{16}\sin^2 2\phi]$
Isotropic	C_{11}

Table 7. Effective Nonlinear Coefficient for Third-Order Interactions, Neglecting Dispersion (sssf Interactions)

Crystal Class	C_{eff}
Trigonal (3 and $\bar{3}$)	$\sin\theta_m(C_{10}\cos 3\phi + C_{15}\sin 3\phi)$
Trigonal ($3m$, $\bar{3}m$, and 32)	$C_{10}\cos 3\phi\sin\theta_m$
Hexagonal (6, $\bar{6}$, $6/m$, 622, $6mm$, $6/mmm$, and $\bar{6}m2$)	0
Tetragonal (4, $\bar{4}$, and $4/m$)	$-\cos\theta_m[C_{21}\cos 4\phi + \frac{1}{4}\sin 4\phi(3C_{18} - C_{11})]$
Tetragonal ($\bar{4}2m$, 422, $4mm$ and $4/mmm$)	$\frac{1}{4}\cos\theta_m\sin 4\phi(C_{11} - 3C_{18})$
Cubic (23, $m3$, 432, $\bar{4}3m$, and $m3m$)	$\frac{1}{4}\cos\theta_m\sin 4\phi(C_{11} - 3C_{16})$
Isotropic	0

Table 8. Effective Nonlinear Coefficient for Third-Order Interactions, Neglecting Dispersion (ssff Interactions)

Crystal Class	C_{eff}
Trigonal (3 and $\bar{3}$)	$\frac{1}{3}C_{11}\cos^2\theta_m + C_{16}\sin^2\theta_m + \sin 2\theta_m \times (C_{10}\sin 3\phi - C_{15}\cos 3\phi)$
Trigonal ($3m$, $\bar{3}m$, and 32)	$\frac{1}{3}C_{11}\cos^2\theta_m + C_{16}\sin^2\theta_m + C_{10}\sin 2\theta_m\sin 3\phi$
Hexgonal (6, $\bar{6}$, $6/m$, 622, $6mm$, $6/mmm$, and $6m2$)	$\frac{1}{3}C_{11}\cos^2\theta_m + C_{16}\sin^2\theta_m$
Tetragonal (4, $\bar{4}$, and $4/m$)	$\frac{1}{2}\cos^2\theta_m[C_{11}\sin^2 2\phi + C_{18}(3\cos^2 2\phi - 1) - 2C_{21}\sin 4\phi] + C_{16}\sin^2\theta_m$
Tetragonal ($\bar{4}2m$, 422, $4mm$, and $4/mmm$)	$\frac{1}{2}\cos^2\theta_m[C_{11}\sin^2 2\phi + C_{18}(3\cos^2 2\phi - 1)] + C_{16}\sin^2\theta_m$
Cubic (23, $m3$, 432, $\bar{4}3m$, and $m3m$)	$\frac{1}{2}\cos^2\theta_m[C_{11}\sin^2 2\phi + C_{16}(3\cos^2 2\phi - 1)] + C_{16}\sin^2\theta_m$
Isotropic	$\frac{1}{3}C_{11}$

Since the dispersion of even the second-order susceptibility is unknown and has been neglected (i.e., Kleinman symmetry has been assumed), only the polarization directions involved will affect the effective coupling for each interaction, independent of wavelength (or order in Table 1). Therefore the effective nonlinear coefficient will need to be calculated for only the following interactions: sss, ssf, sff, fff, sssf, ssff, and sfff. The coefficients for the first four second-order interactions in all uniaxial crystal classes are presented in Tables 2–5. These are followed by the effective third-order coupling coefficients in Tables 6–10, along with coefficients for the interactions ssss and ffff for completeness. Similar, but much more complicated formulas can also be obtained for biaxial crystal classes.

Table 9. Effective Nonlinear Coefficient for Third-Order Interactions, Neglecting Dispersion (sfff Interactions)

Crystal Class	C_{eff}
Trigonal (3 and $\bar{3}$)	$-3\cos^2\theta_m \sin\theta_m (C_{10}\cos 3\phi + C_{15}\sin 3\phi)$
Trigonal ($3m$, $\bar{3}m$, and 32)	$-C_{10}\cos^2\theta_m \sin\theta_m \cos 3\phi$
Hexagonal (6, $\bar{6}$, $6/m$, 622, $6mm$, $6/mmm$, and $\bar{6}m2$)	0
Tetragonal (4, $\bar{4}$, and $4/m$)	$\cos^3\theta_m[C_{21}\cos 4\phi + \frac{1}{4}\sin 4\phi(3C_{18} - C_1)]$
Tetragonal ($\bar{4}2m$, 422, $4mm$, and $4/mmm$)	$\frac{1}{4}(3C_{18} - C_{11})\cos^3\theta_m \sin 4\phi$
Cubic (23, $m3$, 432, $\bar{4}3m$, and $m3m$)	$\frac{1}{4}(3C_{16} - C_{11})\cos^3\theta_m \sin 4\phi$
Isotropic	0

Table 10. Effective Nonlinear Coefficient for Third-Order Interactions, Neglecting Dispersion (ffff Interactions)

Crystal Class	C_{eff}
Trigonal (3 and $\bar{3}$)	$4\sin\theta_m\cos^3\theta_m(C_{15}\cos 3\phi - C_{10}\sin 3\phi) + C_{11}\cos^4\theta_m + \frac{3}{2}C_{16}\sin^2 2\theta_m + C_{33}\sin^4\theta_m$
Trigonal ($3m$, $\bar{3}m$, and 32)	$-4C_{10}\sin\theta_m\cos^3\theta_m\sin 3\phi + C_{11}\cos^4\theta_m + \frac{3}{2}C_{16}\sin^2 2\theta_m + C_{33}\sin^4\theta_m$
Hexagonal (6, $\bar{6}$, $6/m$, 622, $6mm$, $6/mmm$, and $\bar{6}m2$)	$C_{11}\cos^4\theta_m + \frac{3}{2}C_{16}\sin^2 2\theta_m + C_{33}\sin^4\theta_m$
Tetragonal (4, $\bar{4}$, and $4/m$)	$\cos^4\theta_m[\frac{1}{4}C_{11}(3+\cos 4\phi) + \frac{3}{2}C_{18}\sin^2 2\phi + 2C_{21}\sin 4\phi] + \frac{3}{2}C_{16}\sin^2 2\theta_m + C_{33}\sin^4\theta_m$
Tetragonal ($\bar{4}2m$, 422, $4mm$, and $4/mmm$)	$\frac{1}{4}C_{11}\cos^4\theta_m(3+\cos 4\phi) + \frac{3}{2}C_{16}\sin^2 2\theta_m + \frac{3}{2}C_{18}\cos^4\theta_m\sin^2 2\phi + C_{33}\sin^4\theta_m$
Cubic (23, $m3$, 432, $\bar{4}3m$, and $m3m$)	$\frac{1}{4}C_{11}[\cos^4\theta_m(3+\cos 4\phi) + \sin^4\theta_m] + \frac{3}{2}C_{16}[\sin^2 2\theta_m + \cos^4\theta_m\sin^2 2\phi]$
Isotropic	C_{11}

B Third-Harmonic Generation in BBO

As mentioned previously, other groups have attempted to determine the contribution to THG of the cascaded, second-order processes through measurement of the conversion efficiency. In these cases, experimental uncertainties have made a definite assignment of the relative importance of each of the processes impossible. However, we were able to use differences in angular dependence of the cascaded and third-order processes to measure directly the contribution of each to the generated third-harmonic wave.[20]

Before proceeding, it is necessary to define the form of $\chi_{ij}^{(3)}$. The material BBO is of the crystal class $3m$. However, there is some discrepancy concerning the choice of x and y axes in the literature (they are occasionally reversed).[21] For all other uniaxial classes this is unimportant under Kleinman symmetry conditions because both d_{ij} and C_{ij} are isometric on interchange of x and y. However, class $3m$ is not; the Institute of Radio Engineers/Institute of Electrical and Electronics Engineers (IRE/IEEE) standard[22,23] defines the axes so that $d_{11} = 0$ and $d_{22} \neq 0$ (x is perpendicular to a mirror plane). The matter is also confused with regard to the third-order susceptibility. Butcher[24] gives the nonzero tensor elements for linear, second-order, and third-order tensor elements due to crystal-symmetry requirements. These calculations were later corrected by Zhao[25] for classes $\bar{4}2m$, 422, $4mm$, $4/mmm$, 3, $\bar{3}$, 6, $\bar{6}$, and $6/m$, and Shang and Hsu[26] later further corrected 3 and $\bar{3}$ and added corrections for classes $3m$, $\bar{3}m$, and 32. These results have been published in many reference works[16,27,28] along with the forms for d_{ij} that follow the IRE standard.

Unfortunately, the correction Shang and Hsu made to the form for $\chi_{ijkl}^{(3)}$ for classes $3m$, etc., was to define the x and y axes such that y is perpendicular to the mirror plane (m), which does not conform to the IRE standard. This interchange of axes was also made by Yang in pre-

Table 11. Nonzero Third-Order Tensor Elements for Crystal Class $3m$

$zzzz$	
	$xxyy = yyxx$
$xxxx = yyyy$	$xyyx = yxxy$
$= xxyy + xyyx + xyxy$	
	$xyxy = yxyx$
$yyzz = xxzz$	
$zzyy = zzxx$	$yyyz = -yxxz = -xyxz = -xxyz$
$zyyz = zxxz$	$yyzy = -yxzx = -xyzx = -xxzy$
$yzzy = xzzx$	$yzyy = -yzxx = -xzyx = -xzxy$
$yzyz = xzxz$	$zyyy = -zyxx = -zxyx = -zxxy$
$zyzy = zxzx$	

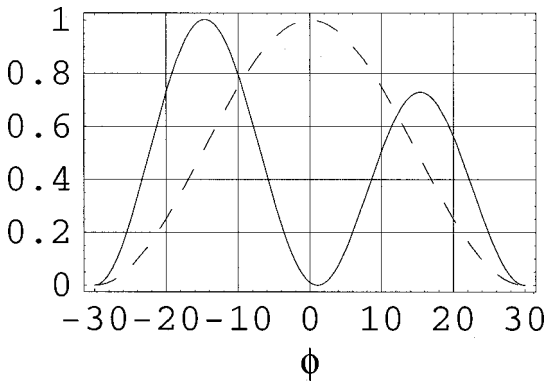

Fig. 2. Dependence of C_{eff}^2 for type I phase matching on azimuthal angle ϕ for second-order interactions only (solid curve) and third-order interactions only (dashed curve). The amplitudes are normalized to unity. For calculating the solid curve, it is assumed that $d_{15}/d_{22} = 0.16/2.2$.[31]

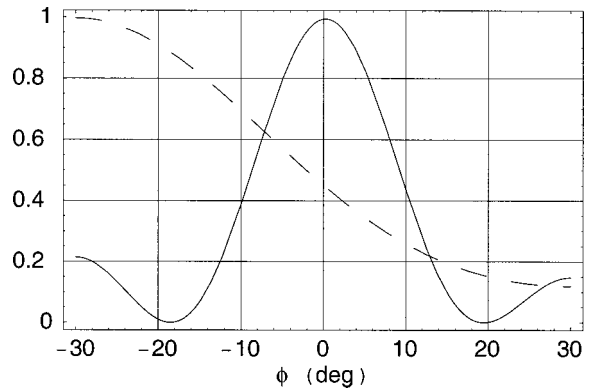

Fig. 3. Dependence of C_{eff}^2 for type II phase matching on azimuthal angle ϕ for second-order interactions only (solid curve) and third-order interactions only (dashed curve). The amplitudes are normalized to unity. In calculating the dashed curve, it is assumed that $C_{11}/3\cos^2\theta_m + C_{16}\sin^2\theta_m = 2C_{10}$ for illustrative purposes.

senting collapsed forms C_{ij} for all crystal classes.[29] In order to be consistent with the reference frame used for $\chi_{ij}^{(2)}$ and to conform to the IRE standard, the original form given by Butcher should be used. This inconsistency in definition is not critical in and of itself, but when both second- and third-order effects play an important role, the same reference frame must be used. The correct form for $\chi^{(3)}$ for crystal class $3m$ in the IRE standard reference frame is then given in Table 11. If Kleinman symmetry is assumed, the collapsed form of the third-order tensor is of the form[30]

$$\mathbb{C} = \begin{bmatrix} C_{11} & 0 & 0 & 0 & 0 & C_{16} & 0 & C_{11}/3 & 0 & C_{10} \\ 0 & C_{11} & 0 & C_{16} & -C_{10} & 0 & C_{10} & 0 & C_{11}/3 & 0 \\ 0 & -C_{10} & C_{33} & 0 & C_{16} & 0 & C_{16} & 0 & C_{10} & 0 \end{bmatrix}. \tag{20}$$

With a consistent reference frame for second- and third-order interactions it is now possible to produce an expression for the effective nonlinear coefficient for THG in BBO. For type I phase matching,

$$C_{\text{eff}} = \frac{2\pi}{\lambda_{2\omega_0}} d_{22}\left[d_{22}\frac{\sin 6\phi}{2}\left(\frac{\cos\theta_m}{n_3\Delta k_7} - \frac{\cos^3\theta_m}{n_4\Delta k_5}\right) + d_{15}\cos 3\phi\left(\frac{\cos^2\theta_m \sin\theta_m}{n_4\Delta k_5} - \frac{\sin\theta_m}{n_3\Delta k_7}\right)\right] + C_{10}\cos 3\phi \sin\theta_m . \tag{21}$$

The equivalent expression for type II phase matching is

$$\begin{aligned} C_{\text{eff}} = \frac{2\pi}{\lambda_{2\omega_0}}\Bigg\{ & d_{22}^2\Bigg[\cos^2 3\phi\left(2\frac{\cos^4\theta_m}{n_4\Delta k_5} - \frac{\cos^2\theta_m}{n_3\Delta k_8}\right) \\ & + \sin^2 3\phi\left(2\frac{\cos^2\theta_m}{n_3\Delta k_7} - \frac{\cos^4\theta_m}{n_4\Delta k_6}\right)\Bigg] \\ & - 2d_{22}d_{15}\sin 3\phi\left(\frac{\sin\theta_m\cos^3\theta_m}{n_4\Delta k_6} + \frac{\sin 2\theta_m}{n_3\Delta k_7}\right) \\ & + d_{15}^2\sin^2\theta_m\left(3\frac{\cos^2\theta_m}{n_4\Delta k_6} + \frac{2}{n_4\Delta k_5}\right) \\ & + \frac{d_{33}}{n_4\Delta k_6}(-d_{22}\sin 3\phi\cos\theta_m\sin^3\theta_m \\ & + d_{15}\sin^4\theta_m)\Bigg\} + 3\left(\frac{C_{11}}{3}\cos^2\theta_m + C_{16}\sin^2\theta_m \right. \\ & \left. + C_{10}\sin 2\theta_m \sin 3\phi\right). \end{aligned} \tag{22}$$

The terms Δk_j are defined as before, and $n_3 = n_{2\omega_0}^o$ and $n_4 = n_{2\omega_0}^e(\theta_m)$ (BBO is a negative uniaxial crystal so that the slow axis is the ordinary axis). Particularly for type I phase matching, the difference in azimuthal angular dependence between second-order and third-order interactions is significant. This can be exploited to determine the relative magnitudes of the two types of interactions in single-crystal THG. The situation is somewhat more complicated for type II phase matching because the angular dependences are not so distinct. However, for both type I and type II phase matching, the azimuthal dependences of the second-order interactions and the third-order interactions are distinct. This distinction is illustrated in Figs. 2 and 3, which show the azimuthal angular dependence of $C_{\text{eff}}^2 \propto I_{3\omega}/I_\omega^3$ for type I and type II phase matching, respectively.

1. *Type I Phase Matching*

The crystal used to measure the azimuthal dependence of the effective coupling coefficient was cut at $\theta_m = 39.03°$ and $\phi = 0°$. The phase matching angles for type I and type II THG at 1053 nm are 37.7° and 47.1°, respectively. The angles for type I and type II SHG are 23.0° and 32.8°, respectively, while that for SFG ($eo \rightarrow e$) is 38.6°. The crystal has a length of 3.31 mm and was solgel antireflection coated at the input for 1053-nm (at normal incidence) and at the output for 351-nm light. The reflections from the input face are in the range of 1%–2% but should be fairly insensitive to input angle within the range of use (<15°–20° from surface normal).

An aperture of 4-mm diameter was placed directly in front of the crystal in order to ensure that the decreasing crystal aperture as the crystal was rotated had no effect on the measurement (see Fig. 4). The azimuthal angle was scanned with a goniometer from −22° to +22° in 1° increments, and the energy $\mathcal{E}_{3\omega}/\mathcal{E}_\omega^3 \propto I_{3\omega}/I_\omega^3$ was measured at each step (Fig. 5). This was done at both 4-mJ input energy and at 8-mJ input energy with the same results. This indicates that we are still operating in the low-drive regime, i.e., $\mathcal{E}_{3\omega} \propto \mathcal{E}_\omega^3$. Approximately 10–20

measurements were taken at each angle at 10 Hz. This was then converted to the internal angle with Snell's law $\phi_{\text{int}} = \sin^{-1}[(\sin \phi_{\text{ext}})/n_5]$. Because the crystal axis (which is the axis of rotation) is not perpendicular to the surface normal, the change of angle of incidence with change in ϕ_{ext} is fairly involved, and use of Snell's law is not perfectly accurate. However, performing the necessary coordinate transformations and rotations shows that use of Snell's law gives the internal angle to within 1% over the range of interest.

The spread in the nonlinear coupling at each value of ϕ is most likely due to small random variations in the pointing of the laser beam. Not only will this change the portion of the beam passing through the limiting aperture, but it will also cause slight fluctuations in the phase-matching angle. In addition to systematic errors, there will also be some uncertainty because as ϕ is changed, the refraction at the surface also causes θ_m to change slightly. At each ϕ the phase-matching angle must be reoptimized, which can result in slight random errors at each angle ϕ.

To relate the values measured for the effective coupling to C_{eff}^2 directly, precise values of the pulse length and beam size would need to be known as well as the interaction length. Fortunately, it is not necessary to know the intensities in order to determine the relative contributions to C_{eff} from second- and third-order interactions. In the low-drive regime the beam sizes, pulse lengths, and interaction lengths simply are an overall multiplicative constant, i.e., $I_5/I_1^3 = AC_{\text{eff}}^2$. Then the nonlinear coupling C_{eff}^2 for type I phase matching shown in Fig. 5 can be expressed as

$$AC_{\text{eff}}^2 = \frac{I_{3\omega}}{I_{\omega}^3} = A\left(\frac{2\pi}{\lambda_{2\omega_0}}\left\{d_{22}^2\frac{\sin 6\phi}{2}\left(\frac{\cos\theta_m}{n_3\Delta k_7} - \frac{\cos^3\theta_m}{n_4\Delta k_5}\right) + \cos 3\phi\left[d_{22}d_{15}\left(\frac{\cos^2\theta_m \sin\theta_m}{n_4\Delta k_5} - \frac{\sin\theta_m}{n_3\Delta k_7}\right)\right]\right\} + C_{10}\sin\theta_m\cos 3\phi\right)^2 \quad (23)$$

$$= A[-83.6\,\text{pm}^2/\text{V}^2 \sin 6\phi + (0.61C_{10} + 9.36\,\text{pm}^2/\text{V}^2)\cos 3\phi]^2, \quad (24)$$

where $\Delta k_5 = k_{3\omega}^e - k_{2\omega}^e - k_{\omega}^o = 3300\,\text{cm}^{-1}$, $\Delta k_7 = k_{3\omega}^e - k_{2\omega}^o - k_{\omega}^o = -2400\,\text{cm}^{-1}$, $n_3 = n_{2\omega}^o = 1.6755$, and $n_4 = n_{2\omega}^e = 1.6277$. Here, values of $d_{22} = 2.2$ pm/V and $d_{15} = 0.16$ pm/V (Ref. 31) are used for the second-order susceptibility and $\theta_m = 37.7°$. It is possible that the origin for ϕ is slightly off because the crystal c axis was not oriented precisely parallel to the table surface. Therefore Eq. (24) is an equation with three unknown parameters: A, C_{10}, and ϕ_0 [ϕ in Eq. (24) becomes $(\phi - \phi_0)$] with A just a scaling factor and ϕ_0 giving the origin. A least-squares fit of Eq. (24) is shown as the solid curve in Fig. 5. This resulted in values of $A = 0.4$, $\phi_0 = -1°$, and $0.61C_{10} + 9.36\,\text{pm}^2/\text{V}^2 = -1.8\,\text{pm}^2/\text{V}^2$. This then gives a value for C_{10} of $-1.8 \pm 0.3 \times 10^{-23}\,\text{m}^2/\text{V}^2$. The value obtained is sensitive to the value of zero for ϕ, which is the main source of uncertainty. The light generated by the cascaded second-order process at $\phi = 15°$ is 50–60 times that generated from the third-order process.

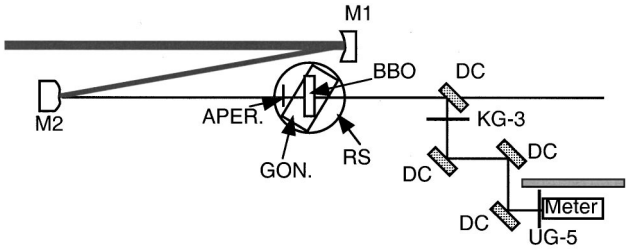

Fig. 4. Experimental setup for measurement of THG. M1 and M2 are a concave/convex mirror pair to down collimate the beam, RS denotes a rotation stage, GON denotes a goniometer with the axis of rotation parallel to the c axis, APER denotes the 4-mm aperture, KG-3 is KG-3 filter glass, UG-5 is UG-5 filter glass, DC are four dichroic mirrors, and Meter is a pyroelectric energy meter.

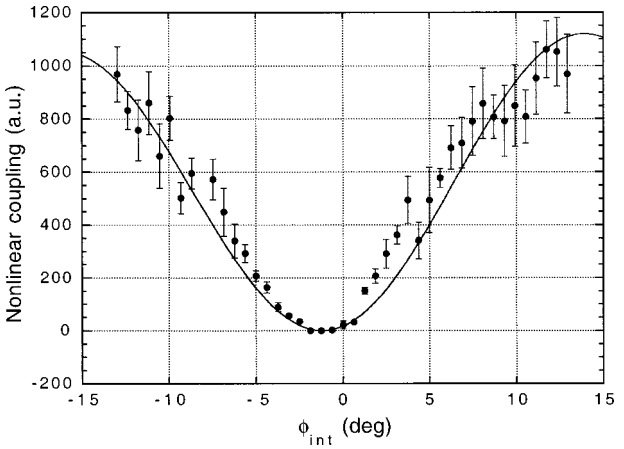

Fig. 5. Effective nonlinear coupling as a function of internal azimuthal angle ϕ_{int} in BBO. The solid curve is a fit with known values for second-order coefficients.

It should be noted that there is some discrepancy in the reported magnitudes for d_{31} for BBO (ranging from 0.02 to 0.16 pm/V)[31–34] and recently, experiments were done indicating that $d_{22}/d_{31} < 0$, i.e., they are of opposite sign.[35] This range of d_{31} gives a range for C_{10} from 0.4 to $-1.8 \times 10^{-23}\,\text{m}^2/\text{V}^2$. Tomov *et al.*[9] give a value of $10^{-22}\,\text{m}^2/\text{V}^2$ for C_{10} and state that, for type I phase matching, the third-order nonlinearity is the dominant coupling mechanism. This is in strong conflict with the data measured here. The advantage of this technique for measuring the third-order susceptibility tensor elements is that it is not necessary to have an accurate knowledge of the intensity of the beams involved, only an accurate knowledge of the angles. The uncertainty in C_{10} then rests mainly with uncertainty in the values for the second-order susceptibilities.

2. *Type II Phase Matching in BBO*

By rotating the phase-matching angle of the BBO crystal by 10°, it was possible to repeat this experiment for type II phase matching ($\theta_m = 47.1°$). However, as was mentioned before, using the form of C_{eff} [Eq. (22)] for type II configurations is more complex. Also, a simplification may be made since it is known that for BBO

$d_{15} < 0.1 d_{22}$, so all terms with d_{15}^2 may be neglected. Grouping terms by azimuthal dependence gives

$$KC_{\text{eff}}^2 = \frac{I_5}{I_\omega^3} = K\Big[Ad_{22}^2\cos^2 3\phi + Bd_{22}^2\sin^2 3\phi + \sin 3\phi(Dd_{22}d_{15} + Ed_{22}d_{33} + C_{10}\sin 2\theta_m) + Fd_{33}d_{15} + \left(\frac{C_{11}}{3}\cos^2\theta_m + C_{16}\sin^2\theta_m\right)\Big]^2, \tag{25}$$

where

$$A = \frac{2\pi}{3\lambda_{2\omega_0}}\left(2\frac{\cos^4\theta_m}{n_4\Delta k_5} - \frac{\cos^2\theta_m}{n_3\Delta k_8}\right) = 10.3,$$

$$B = \frac{2\pi}{3\lambda_{2\omega_0}}\left(2\frac{\cos^2\theta_m}{n_3\Delta k_7} - \frac{\cos^4\theta_m}{n_4\Delta k_6}\right) = -4.50,$$

$$D = -2\frac{2\pi}{3\lambda_{2\omega_0}}\left(\frac{\sin\theta_m\cos^3\theta_m}{n_4\Delta k_6} + \frac{\sin 2\theta_m}{n_3\Delta k_7}\right) = 5.64,$$

$$e = -\frac{2\pi}{3\lambda_{2\omega_0}}\frac{\sin^3\theta_m\cos\theta_m}{n_4\Delta k_6} = -1.17,$$

$$F = \frac{2\pi}{3\lambda_{2\omega_0}}\frac{\sin^4\theta_m}{n_4\Delta k_6} = 1.26. \tag{26}$$

where $\Delta k_5 = k_{3\omega}^e - k_{2\omega}^e - k_\omega^o = 1870\,\text{cm}^{-1}$, $\Delta k_6 = k_{3\omega}^e - k_{2\omega}^e - k_\omega^e = 5650\,\text{cm}^{-1}$, $\Delta k_7 = k_{3\omega}^e - k_{2\omega}^o - k_\omega^o = 6180\,\text{cm}^{-1}$, $\Delta k_8 = k_{3\omega}^e - k_{2\omega}^o - k_\omega^e = -2400\,\text{cm}^{-1}$, $n_3 = n_{2\omega}^o = 1.6755$, and $n_4 = n_{2\omega}^e = 1.6080$.

Now, C_{10} is known from the type I measurement (same crystal is being used), as is ϕ_0, so the only unknowns in Eq. (25) are C_{11} and C_{16}. There is no way to distinguish between C_{11} and C_{16}. The data obtained are shown in Fig. 6 along with the fit obtained with Eq. (25) and the value for d_{ij} from Ref. 31; d_{33} was used as a fit parameter in this case. The fit parameters obtained are $K = 0.10$, $d_{33} = 1.7\,\text{pm/V}$, and $C_{11}(\cos^2\theta_m)/3 + C_{16}\sin^2\theta_m = 4.0 \pm 0.2 \times 10^{-23}\,\text{m}^2/\text{V}^2$. The value obtained for d_{33} is sensitive to values used for d_{15} and small errors in ϕ_0 and can range from 1 to 5 pm/V. If, instead, the values for d_{ij} from Ref. 34 are used (with $d_{22} = 2.2\,\text{pm/V}$, $d_{15} = 0.026\,\text{pm/V}$, and $d_{33} = 0.04\,\text{pm/V}$, as well as $C_{10} = -6 \times 10^{-24}\,\text{m}^2/\text{V}^2$), a nearly identical fit is obtained if the input angle is allowed to vary by 0.3°, which is within the margin of error for ϕ_0. As a note of caution, the equations for C_{eff} in this section assume Kleinman symmetry for which $d_{31} = d_{15}$, which is not consistent with the values of Shoji *et al.* of $d_{31} = 0.04\,\text{pm/V}$ and $d_{15} = 0.026\,\text{pm/V}$.

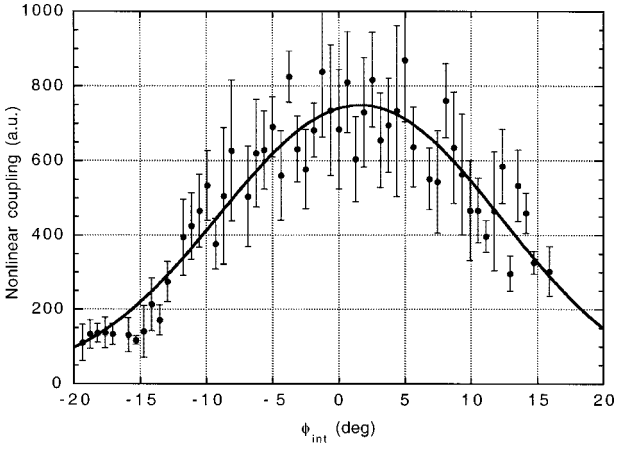

Fig. 6. Effective nonlinear coupling as a function of internal azimuthal angle ϕ_{int} in BBO. The solid curve is a fit with known values for second-order coefficients.

However, irrespective of the sensivity of these parameters to small errors in the fit, the value for the third-order tensor elements is not affected by such variations; in all cases the value of $C_{11}(\cos^2\theta_m)/3 + C_{16}\sin^2\theta_m$ is $4.0 \pm 0.2 \times 10^{-23}\,\text{m}^2/\text{V}^2$. This value agrees with the range given by Tomov *et al.* of $2-8 \times 10^{-23}\,\text{m}^2/\text{V}^2$ and is on the low end of that given by Qui and Penzkofer of $6.4 \times 2.8 \times 10^{-23}\,\text{m}^2/\text{V}^2$. However, the level of 1% conversion efficiency is not reached until 80 GW/cm^2, compared with 50 GW/cm^2 as reported by Qiu and Penzkofer.

4. NUMERICAL SOLUTION OF COUPLED-WAVE EQUATION

The system of equations (1)–(5) of course cannot be solved analytically, and so numerical techniques must be used. This we have done using all three spatial dimensions plus time and have used the results to verify computationally the effect of cascaded second-order processes on the THG. We have also analyzed the maximum conversion efficiencies achievable at input intensities up to 1 TW/cm^2. Finally, we discuss the factors that will limit the conversion efficiencies to less than 50%.

A. Numerical Algorithm

One algorithm that is commonly used to solve this sort of system is known as the beam propagation method or the split-step method.[36–39] The right-hand sides of Eqs. (1)–(5) are separated into a dispersive/diffractive part (all terms involving time and space derivatives) and a nonlinear part. Expressed in operator notation, this means that

$$\frac{\partial A_j}{\partial z} = (\mathbb{D}_j + \mathbb{N}_{1j})A_j + \mathbb{N}_{2j}, \tag{27}$$

where

$$\mathbb{D}_j = -\beta_{1j}\frac{\partial}{\partial t} - \frac{i}{2}\beta_{2j}\frac{\partial^2}{\partial t^2} + \frac{i}{2k_j}\nabla_\perp^2, \tag{28}$$

and, for example,

$$\mathbb{N}_{11} = \frac{i\omega_1}{n_1 c}\left(\frac{3C_1^{\text{SPM}}}{2}|A_1|^2 + 3C_1^{\text{XPM}}|A_5|^2 + 3C_2^{\text{XPM}}|A_2|^2\right), \tag{29}$$

$$\mathbb{N}_{21} = \frac{i\omega_1}{n_1 c}\Big[d_1 A_3 A_1^* \exp(i\Delta k_1 z) + d_3 A_4 A_1^* \exp(i\Delta k_3 z) + d_2 A_3 A_2^* \exp(i\Delta k_2 z) + d_4 A_4 A_2^* \exp(i\Delta k_4 z) + d_5 A_5 A_4^* \exp(i\Delta k_5 z) + d_7 A_5 A_3^* \exp(i\Delta k_7 z) + 3C_1 A_5 A_2^* A_1^* \exp(i\Delta k_{11} z) + \frac{3C_2}{2} A_5 A_1^{*2} \exp(i\Delta k_{12} z) + \frac{3C_3}{2} A_5 A_2^{*2} \exp(i\Delta k_{13} z)\Big]. \quad (30)$$

These two classes of operations are assumed to function independently for an appropriate choice of the z interval Δz. Equation (27) can then be split into three equations that can be solved independently:

$$\frac{\partial A_j}{\partial z} = \mathbb{D} A_j, \quad (31)$$

$$\frac{\partial A_j}{\partial z} = \mathbb{N}_{1j} A_j, \quad (32)$$

$$\frac{\partial A_j}{\partial z} = \mathbb{N}_{2j}. \quad (33)$$

The dispersive/diffractive step can be solved easily by moving to Fourier space and replacing $\partial/\partial x_j$ with ik_{x_j} and $\partial/\partial t$ with $-i\omega_0$. Then

$$A_j^{(n+1)} = \mathcal{F}^{-1}\{\exp[\mathbb{D}_j(\omega, \mathbf{k})\Delta z]\mathcal{F}[A_j^{(n)}]\}, \quad (34)$$

where the superscript (n) in parentheses denotes the step n, and the dispersive operator $\mathbb{D}_j(\omega, \mathbf{k})$ in Fourier space is

$$\mathbb{D}_j(\omega, \mathbf{k}) = i\omega\beta_{1j} + \frac{i}{2}\omega^2\beta_{2j} - \frac{i}{2k_j}(k_{jx}^2 + k_{jy}^2). \quad (35)$$

The nonlinear part is handled in real space with Eq. (32), giving rise to a simple exponential solution $A_j^{(n+1)} = \exp(\mathbb{N}_{1j}\Delta z)A_j^{(n)}$. However, the solution of the coupled set of equations of the form of Eq. (33) must be done with some sort of numerical technique such as Runge–Kutta. It was found that second-order Runge–Kutta was adequate, which utilizes the following difference equation:

$$y^{(n+1)} = y^{(n)} + \Delta z f\left[z^{(n)} + \Delta z/2,\ y^{(n)} + \frac{\Delta^2}{2} f(z^{(n)},\ y^{(n)})\right]. \quad (36)$$

Finally, by splitting the dispersive operation into two half-steps (over an interval $\Delta z/2$), one before the nonlinear operation and one after, the overall operation (dispersive and nonlinear parts) becomes unitary, and the accuracy of the method is improved. This is known as the symmetrized or symmetric split-step method.[37,40]

B. Calculated Third-Harmonic Generation and Maximum Efficiency

It was found that even four-dimensional calculations (with a $64 \times 64 \times 64$ grid and a few tens of z steps) could be run for a typical crystal in a few minutes on a fast workstation if the second-order coupling terms were set to 0. However, the inclusion of these terms in THG calculations, because they are not phase matched, introduces a rapidly oscillating component in addition to the slowly varying third-harmonic wave, i.e., it becomes a stiff set of equations. This requires the step size in z to be reduced greatly (by as much as a factor of 100). The calculation times correspondingly increase to a few hours for crystals of a few millimeters thickness. An illustration of this in the small-signal growth of the second- and third-harmonic waves is shown in Fig. 7. If the interaction is due only to a third-order nonlinearity, the growth with propagation distance is smooth and is simply proportional to z^2, as expected. However, if the THG is due solely to a second-order nonlinear coupling, the growth of the third-harmonic wave is modulated due to the periodic behavior of the intermediate second-harmonic waves. The step

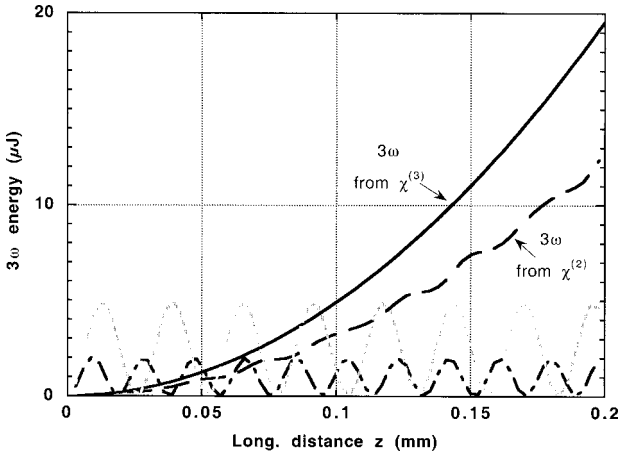

Fig. 7. Calculated amplitudes of electric field envelope functions A_j as a function of propagation distance in BBO crystal. The solid curve shows what would be expected for the third harmonic in the presence of $\chi^{(3)}$ only, and the dashed curve shows the expected behavior for the third harmonic in the presence of $\chi^{(2)}$ only. The dotted and dash-dotted curves are the ordinary and extraordinary second-harmonic waves, respectively.

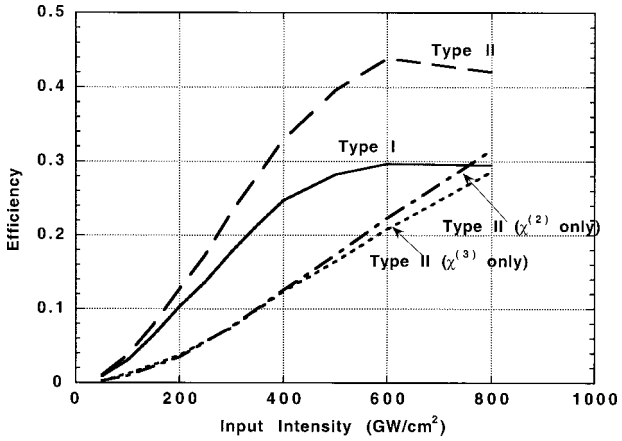

Fig. 8. Predicted conversion efficiency in a 1-mm crystal of BBO for both type I and type II phase matching. The dotted curve is for calculation done for type II phase matching with no cascaded process allowed. The dash-dotted curve is the calculated conversion efficiency with no third-order coupling, i.e., only cascaded interactions one allowed.

size used in the calculations must be smaller than this short scale-length variation.

As these calculations are extended to higher intensities, we observe that the conversion efficiency saturates for input irradiances $>500\,\mathrm{GW/cm^2}$. Such calculations that use the values for $\chi^{(3)}$ measured are graphed in Fig. 8 for type I and type II phase matching assuming a flattop spatial profile of 5-mm diameter and a Gaussian temporal profile of 400 fs. The calculations also include values for $C_{2,3,4,5}^{\mathrm{SPM}}$ of $10^{-22}\,\mathrm{m^2/V^2}$ for both fundamental waves and for C_1^{SPM} of $1.3 \times 10^{-22}\,\mathrm{m^2/V^2}$ for the third-harmonic wave. The cross-phase modulation terms were assumed to be zero, mainly because there are no reliable data for these terms. The values reported for the nonlinear refractive index γ are $\sim 5 \times 10^{-16}\,\mathrm{cm^2/W}$ at 820 nm,[41] or ~ 1.7 times that of potassium dihydrogen phosphate (KDP).

C. Limiting Factors

The curves saturate at approximately 30% and 44% for type I and type II phase matching, respectively, with the main mechanism limiting the efficiency being self-phase modulation (SPM). With the SPM coefficients set to zero, the calculated efficiency peaks in the 60%–70% range. However, the effect, similar to that discussed thus far for THG, is a complex interaction between the second- and third-order coupling. The dotted and dash-dotted curves in Fig. 8 are calculations done with the same parameters, but setting $\chi_{ij}^{(2)}$ and $\chi_{ij}^{(3)}$ to zero, respectively. In either case, when the other processes are neglected, the saturation does not occur until higher efficiency is achieved.

This would indicate that phase-modulation effects at high intensities are quite complicated and can occur through many channels. The square of the final electric field amplitudes and phases of the fundamental and third-harmonic waves calculated for type II phase matching in 1 mm of BBO at 800 $\mathrm{GW/cm^2}$ are shown in Figs. 9–11. Of particular interest is Fig. 10, where no third-order interactions are included in the calculation. Even though the overall process is phase matched, the nonphase-matched intervening second-order processes produce significant modulation of the phase of the fundamental waves (up to 1 rad across the pulse). When SPM is included, the phase modulation becomes very large, particularly in the generated wave. Although at 800 $\mathrm{GW/cm^2}$ the B integral is approximately 1–2 rad for the fundamental waves and should be even smaller for the generated wave, the accumulated phase at the peak of the 3ω pulse is well over 3 rad. This is the case whether or not the second-order interactions are included, suggesting that in the presence of SPM, the phase of the generated harmonics is strongly modulated by the conversion process. Finally, the existence of the second-harmonic channel produces a much more pronounced amplitude modulation on the third harmonic and lowers the maximum achievable intensity.

D. Self-Phase Modulation

However, relating the above analysis to experimental conditions is a complicated issue. First, the individual tensor elements of C_{ij} are not well known for most materials, with usually a value for the nonlinear refractive index n_2 being all that is know. Second, there has been discussion concerning the effect of the dispersion in the nonlinear refractive index on frequency-conversion processes. Finally, self-and cross-phase modulation are themselves phase matched third-order processes that can be affected by contributions of non-phase-matched second-order processes.

Recently, there have been several published papers[42–45] that suggest that the effect of SPM on SHG is actually quite dependent upon the dispersion that exists between the nonlinear refractive index n_2 at the fundamental and the second harmonic (where n_2 is defined by $n = n_0 + n_2|E|^2 = n_0 + \gamma I$). In fact, the value for γ for KD*P has been measured to vary from $2-4 \times 10^{-16}\,\mathrm{cm^2/W}$ from

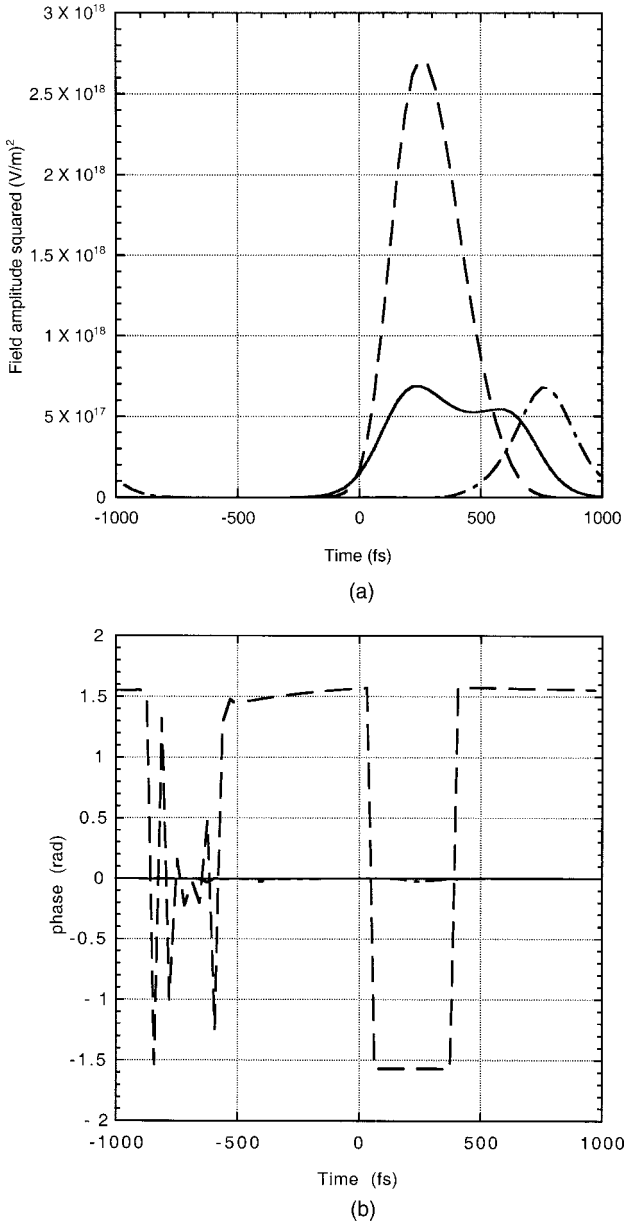

Fig. 9. Calculated square of (a) electric field amplitude and (b) phase at the crystal exit, involving only $\chi^{(3)}$ and no explicit SPM ($C_j^{\mathrm{SPM}} = 0$, $d_j = 0$). Input intensity is 800 $\mathrm{GW/cm^2}$. The solid curve is the ordinary fundamental, the dash-dotted curve is the extraordinary fundamental, and the dashed curve is the third harmonic (extraordinary).

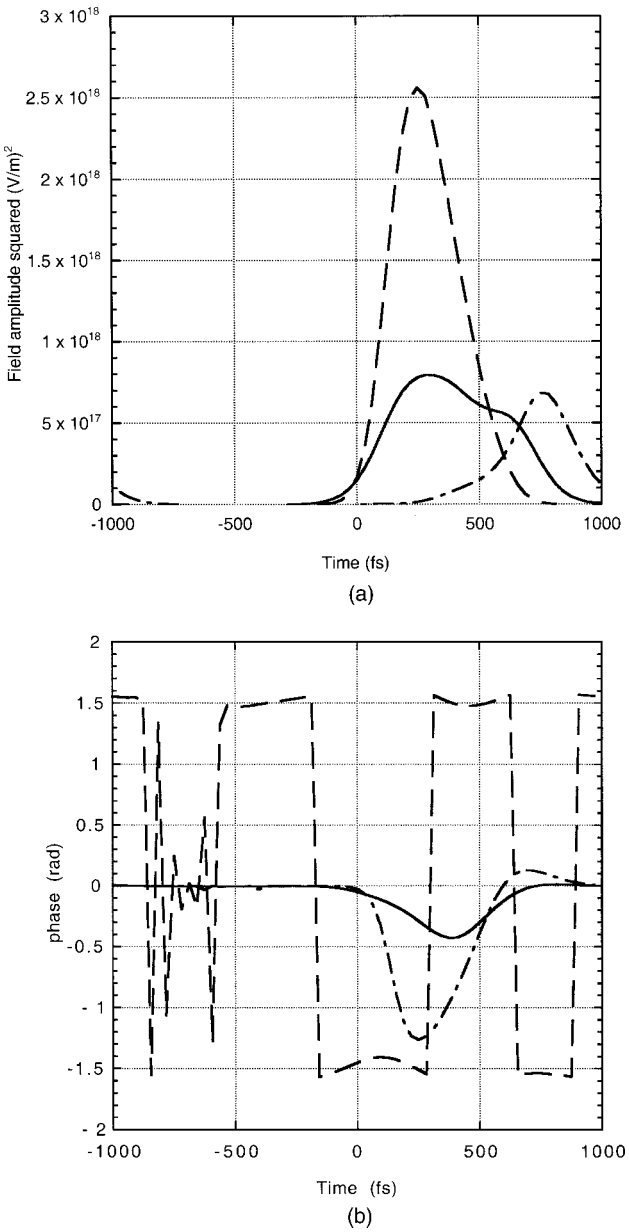

Fig. 10. Calculated square of (a) electric field amplitude and (b) phase at the crystal exit involving only $\chi^{(2)}$ and $\chi^{(3)}$ with no explicit SPM ($C_j^{\mathrm{SPM}} = 0$). Input intensity is 800 GW/cm^2. The solid curve is the ordinary fundamental, the dash-dotted line is the extraordinary fundamental, and the dashed curve is the third harmonic (extraordinary).

1064–400 nm,[46] indicating that significant dispersion exists. The nonlinear refractive index is related to C_{eff} by

$$n_2 = \frac{3C_{\mathrm{eff}}^{\mathrm{SPM}}}{2n_0} = \frac{\epsilon_0 c n_0}{2}\gamma, \tag{37}$$

and so the dispersion of n_2 in SHG is the same as dispersion between $C_{\mathrm{eff}}^{\mathrm{SPM}}(-\omega;\omega,-\omega,\omega)$ and $C_{\mathrm{eff}}^{\mathrm{SPM}}(-2\omega;2\omega,-2\omega,2\omega)$.

There are two points that should be made: first, that as seen in the actual form of C_{eff} for the various interactions, the actual value for C_{eff} is highly dependent on propagation angle, and since the fundamental and second-harmonic waves are typically of different polarizations (e.g., ordinary versus extraordinary), the angular dependence will be different. Even if there is no actual dispersion in the tensor elements, the effective coupling, and thus the value of n_2, is not equal. For example, we shall assume type I SHG in KDP (class $\bar{4}2m$), where $\phi = \pi/4$ and $\theta_m = \pi/4$. Then SPM for the fundamental is an *oooo* interaction, and for the second harmonic, it is an *eeee* interaction. The effective nonlinear coupling is then proportional to

$$C_{1\omega} = \frac{1}{2}(C_{11} + 3C_{18}) \tag{38}$$

for the fundamental and

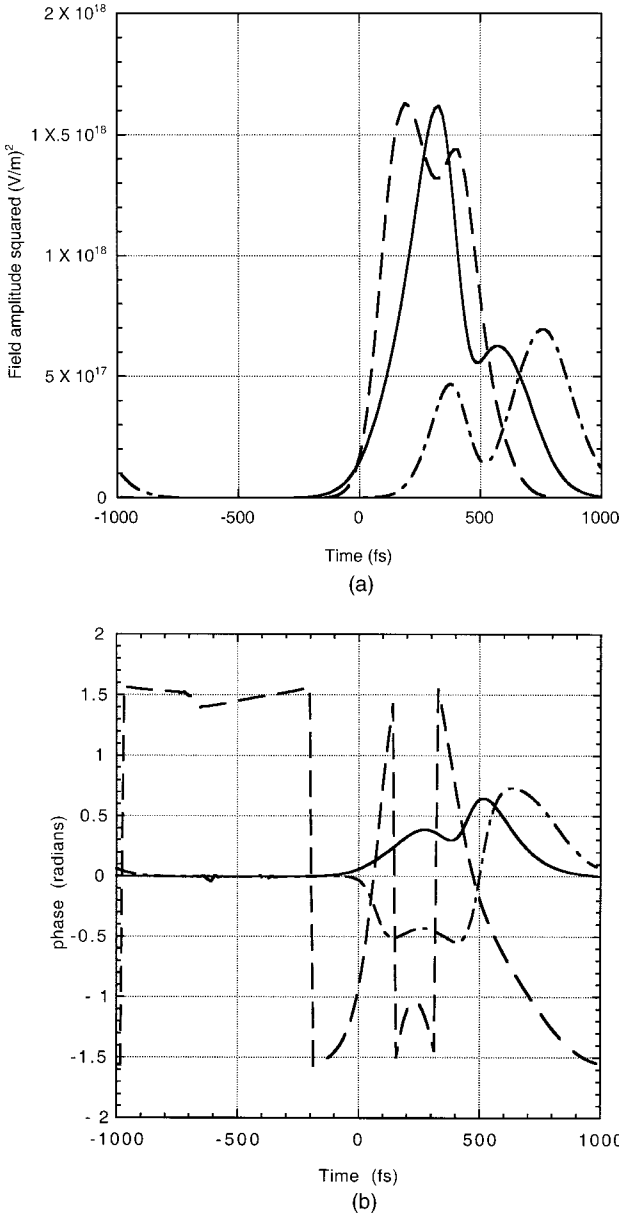

Fig. 11. Calculated square of (a) electric field amplitude and (b) phase at the crystal exit, involving all possible processes. Input intensity is 800 GW/cm^2. The solid curve is the ordinary fundamental, the dash-dotted curve is the extraordinary fundamental, and the dashed curve is the third harmonic (extraordinary).

$$C_{2\omega} = \frac{1}{8}(C_{11} + 3C_{18}) + \frac{C_{33}}{4} + \frac{3C_{16}}{2}$$

$$= \frac{1}{4}C_{1\omega} + \frac{C_{33}}{4} + \frac{3C_{16}}{2} \tag{39}$$

for the second harmonic. It is clear that although the tensor elements are assumed to be independent of wavelength, the values for SPM for the fundamental and second harmonic are formally very different in KDP. The actual difference between Eqs. (38) and (39) is unknown because the tensor elements C_{16} and C_{33} are unknown.

This complicated angular dependence of C_{eff} for SPM (the interaction of a wave with itself) indicates that the nonlinear refractive index must be measured with much greater attention to the crystal orientation than has been done in the literature to this point. It is typically measured for ordinary waves and extraordinary waves at some wavelength, and then this value is used for any crystal orientation. Presumably, this measurement is usually done for $\theta_m = \pi/2$ and $\phi = 0$ (or $\pi/2$). For KDP under these conditions,

$$C_{\text{ord}} = C_{11}, \tag{40}$$

$$C_{\text{ext}} = C_{11} + C_{33}. \tag{41}$$

Second, SPM and XPM are subject to similar cascaded second-order interactions,[41,47–49] as has been discussed concerning third-harmonic generation. Much research has focused on the use of slightly mismatched second-order processes such as SHG to significantly enhance SPM effects. However, all possible interactions of the form $\omega \rightarrow \omega_1 + \omega_2$ followed by $\omega_1 + \omega_2 \rightarrow \omega$ can also contribute to SPM in a similar way, albeit much smaller because of the large phase mismatches that are involved. The sum of the SPM contributions of all such interactions may be large enough to account for a significant fraction of values measured for n_2 and usually assigned to the third-order susceptibility.

The question as to the effect of SPM and XPM on high-intensity frequency conversion is at best a complicated issue. The angular dependence is some mixture of second- and third-order effective coupling coefficients involving an infinite number of non-phase-matched three-wave interactions. Nonetheless, the role that phase modulation effects play on frequency conversion at high intensities is significant.

5. EXPERIMENTAL CONVERSION EFFICIENCY AND LIMITATIONS

We have also made measurements of the third-harmonic conversion efficiency in three materials: BBO, d-LAP, and KD*P. These materials were chosen because they were available and were phase matchable for THG of 1053-nm light. KD*P also has published values of $\chi^{(3)}$ that indicated that efficient THG would be possible. There are many other materials, including ones with small second-order tensor elements, which may prove useful in single-crystal THG of high-intensity lasers.

A. BBO

In addition to the azimuthal measurements in BBO, the energy at 3ω was measured as a function of energy at ω. The corresponding efficiencies at the optimal azimuthal angle are shown in Figs. 12 and 13 as a function of input intensity for type I and type II phase matching, respectively. Up to 6% of the fundamental energy was converted into the third harmonic at an input intensity of 200 GW/cm^2. The fit parameters are 5.33×10^{-11} J/(GW/cm^2)^3 for type I phase matching and 4.45×10^{-11} J/(GW/cm^2)^3 for type II phase matching (4-mm beam size). Again, these measurements were for a clipped Gaussian beam in which efficient conversion occurs only near the center of the beam; better results could be obtained by use of a flattop beam profile.

By comparison, the measured conversion efficiency when the crystal was aligned to be phase matched for SFG ($\theta_m = 38.6°$) was less than 0.01%. This low conversion efficiency for the cascaded process is partially because the experimental arrangement was for type I THG and there was no extraordinary pump wave (this angle is for phase-matched type II SFG). However, numeric calculations indicate that although setting $\theta_m = 38.6°$ increases THG conversion efficiencies 100-fold above the

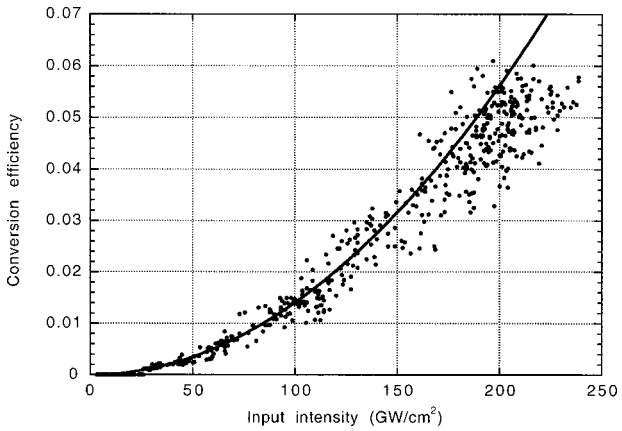

Fig. 12. Conversion efficiency from a single BBO crystal at 351 nm along with a quadratic fit to low-drive points. Type I phase matching with $\phi_{\text{int}} = -15°$.

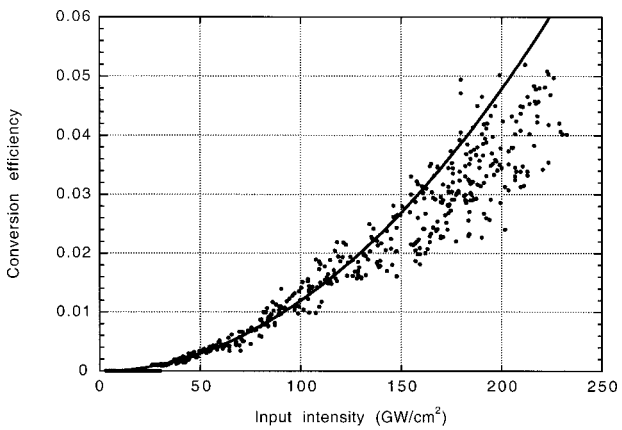

Fig. 13. Conversion efficiency from a single BBO crystal at 351 nm along with a quadratic fit to low-drive points. Type II phase matching ($\phi_{\text{int}} = 0°$).

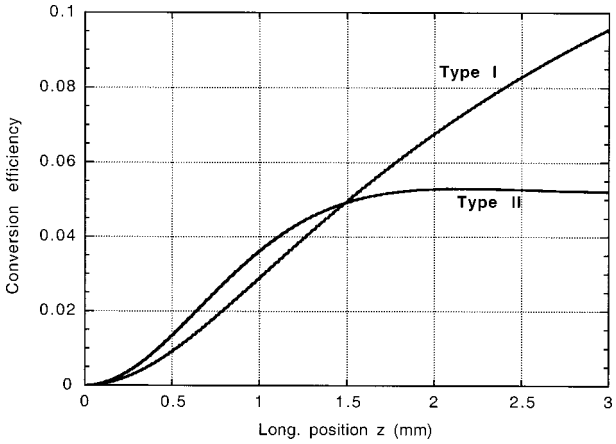

Fig. 14. Calculated longitudinal growth of type I and type II 3ω energies. 350-fs pulses, 200-GW/cm^2 input intensity (8 mJ).

background, the efficiencies for any level of extraordinary pump light remain less than 0.1% for 200-GW/cm^2 input intensity. Apparently, the phase-matched SFG process is not sufficient to allow the efficient transfer of energy to the third-harmonic wave.

Type I phase matching gives better conversion for THG, even though according to the previous calculations, $I_{3\omega} \propto 8.2 \times 10^{-23}\,\mathrm{m}_2/\mathrm{V}^2 I_{\omega,0}^3$ for type I and $\phi = -15°$ and to $I_{3\omega} \propto (4/3)^{1/2}(9.0 \times 10^{-23})\,\mathrm{m}^2/\mathrm{V}^2 I_{\omega,0}^3$ for type II phase matching and $\phi = 0°$. The factor $(4/3)^{1/2}$ is from the degeneracy factor of 3 for type II phase matching coupled with the factor of 4/27 from the initial intensities being divided between the two polarizations of the fundamental. In other words, for type II phase matching, $I_1 = 2I_{\omega,0}/3$ and $I_2 = I_{\omega,0}/3$, where $I_{\omega,0}$ is the input irradiance at 1ω.

Higher conversion efficiency for type I phase matching is possible in this case because of the different group velocities involved in the two different phase-matching configurations. While the interaction length $l_{\mathrm{eff}} = (1/v_{g1} - 1/v_{g2})^{-1}\tau$ due to the group-velocity mismatch between the fundamental ordinary wave and the third-harmonic extraordinary wave is similar for the two configurations (1.2 mm for type I versus 1.7 mm for type II for a 350-fs pulse), the major limiting factor in type II phase matching is the walk-off between the two polarizations of the fundamental beam. These two waves walk off in approximately 1.5 mm, resulting in no further interaction, as can be seen in Fig. 14. For type I phase matching, conversion continues to proceed as the pulses walk off from each other, with the energy simply being added to the tail of the 3ω pulse. This broadens the generated 3ω pulse from 300 fs to 540 fs in this calculation. There is little effect on the 3ω pulse length for the type II interaction. Higher intensities were not investigated because of the onset of gray tracking in the BBO. This was not observed in another crystal that was not phase matched for THG; thus it is likely that the damage is due to the generated UV (which reached up to 40 GW/cm^2).

B. LAP

Similar measurements were done for the deuterated (approximately 95%) organic salt L-arginine phosphate (d-LAP) with formula

$$(\mathrm{H_2N})_2^+\mathrm{CNH(CH_2)_3CH(NH_3)^+COO^-} \cdot \mathrm{H_2PO_4^-} \cdot \mathrm{H_2}.$$

This substance is a biaxial (monoclinic) crystal of point group 2 and transparent from 250 nm to 1300 nm. The crystal of d-LAP available was 1 mm in thickness with a surface normal that was at an angle of 11° with respect to the z axis and lying in the x–z plane. Both faces were polished but uncoated. For propagation in the x–z plane at this angle, symmetry [with an even (second-order) or odd number (third-order) of waves polarized in the y–z plane] requires both second- and third-order coupling to be identically zero for type I THG.

However, type II phase matching is not identically zero in this plane and is possible in d-LAP for 1053-nm light, although some of the cascaded processes involved are identically zero, again from the same symmetry arguments. The effective, nonzero nonlinear coefficients are

$$d_1 = -d_{22}, \tag{42}$$

$$d_4 = d_5 = d_8 = -d_{21}\cos^2\theta_m + d_{36}\sin 2\theta_m - d_{23}\sin^2\theta_m, \tag{43}$$

$$C_1 = C_{18}\cos^2\theta_m + C_{24}\sin^2\theta_m - C_{15}\sin 2\theta_m. \tag{44}$$

Again, there exists a nonstandard reference frame that is sometimes used for class 2 crystals. This nonstandard frame is used by Singh[28] to give the form for C_{ij}. However, C_{ij} in the reference frame following the IRE/IEEE standard is

$$\mathbb{C} = \begin{bmatrix} C_{11} & 0 & C_{13} & 0 & C_{15} & C_{16} & C_{17} & C_{18} & 0 & 0 \\ 0 & C_{22} & 0 & C_{24} & 0 & 0 & 0 & 0 & C_{29} & 0 \\ C_{31} & 0 & C_{33} & 0 & C_{35} & C_{36} & C_{37} & C_{38} & 0 & 0 \end{bmatrix}, \tag{45}$$

and, under Kleinman symmetry conditions, $C_{18} = C_{29}$, $C_{16} = C_{37}$, $C_{24} = C_{35}$, $C_{15} = C_{20} = C_{38}$, $C_{17} = C_{31}$, and $C_{13} = C_{36}$.

The effective coupling is given by

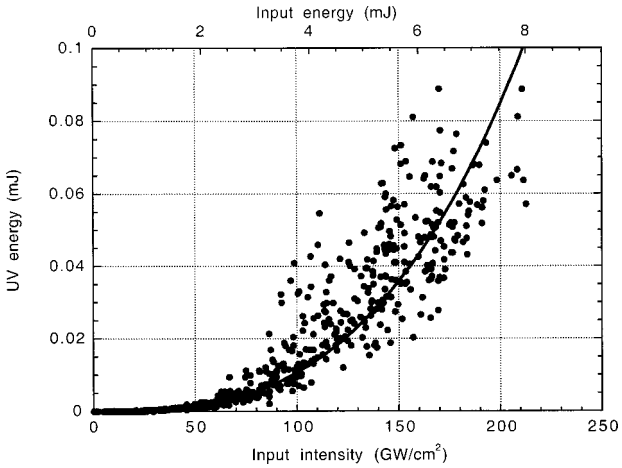

Fig. 15. Measured energy generated at the third harmonic in a 1-mm crystal of d-LAP. The input energy at 200 GW/cm^2 is 8 mJ. Type II phase matching. The curve is a cubic, least-squares fit to data.

$$C_{\text{eff}} = \frac{2\pi}{\lambda_{2\omega_0}}\left(\frac{d_1 d_8}{n_3 \Delta k_8} + 2\frac{d_4 d_5}{n_4 \Delta k_5}\right) + 3C_1. \quad (46)$$

For type II phase matching of 1053-nm light, $\theta_m = 20.2°$, $\Delta k_5 = 1601\,\text{cm}^{-1}$, $\Delta k_8 = -2171\,\text{cm}^{-1}$, $n_4 = 1.5179$, and $n_3 = 1.5768$. For d-LAP, $d_{21} = 0.40$ pm/V, $d_{22} = 0.39$ pm/V, $d_{23} = 0.83$ pm/V, and $d_{36} = -0.59$ pm/V.[50] The conversion efficiency of d-LAP was measured with the aforementioned crystal (Fig. 15) and was found to be ~20% that of type II BBO.

Comparing the conversion of the two crystals is complicated by the BBO crystal being longer (3.1 mm) than the interaction length of BBO, so the exact interaction length is unknown, but l_{eff} is calculated to be approximately 1.5 mm (see Fig. 14). This introduces a factor of 1.5^2 when comparing C_{eff} of the two materials. Therefore

$$C_{\text{eff}}^{\text{d-LAP}} \cong \left(\frac{1.52^2}{5}\right)^{1/2} \cong \frac{2}{\sqrt{5}} C_{\text{eff}}^{\text{BBO}}, \quad (47)$$

and $C_{\text{eff}}^{\text{BBO}} = 9 \times 10^{-23}\,\text{m}^2/\text{V}^2$ for type II phase matching. Then substituting the appropriate values into Eq. (46) and solving for C_1 in Eq. (47) gives a value for C_1 of $4 \times 10^{-23}\,\text{m}^2/\text{V}^2$ for d-LAP. It is interesting to note that although, after accounting for the different interaction lengths, the conversion efficiency in BBO is two times that in d-LAP, the largest $\chi^{(2)}$ tensor element for d-LAP is less than half the largest element for BBO. The d^4 dependence would indicate a possibility of over 16 times the conversion efficiency. However, the larger phase mismatches involved and larger indices of refraction for BBO substantially reduce the cascaded coupling.

C. KD*P

Similar measurements were also made with a 1-mm-thick, 1-in (2.5-cm)-aperture, piece of potassium dideuterium phosphate (KD*P, 99% deuterated, crystal class $\bar{4}2m$) as the medium. Reported values[51] of C_{eff} of up to $10^{-22}\,\text{m}^2/\text{V}^2$ indicated that very efficient single-crystal THG might be possible. Only type I phase matching is possible at 1053 nm (with no phase matching possible at 820 nm), and the relevant effective nonlinear coefficients are given by

$$d_1 = 0, \quad (48)$$

$$d_3 = d_7 = -d_{36}\sin 2\phi \sin\theta_m, \quad (49)$$

$$d_5 = d_{36}\cos 2\phi \sin 2\theta_m, \quad (50)$$

$$C_2 = \frac{1}{4}(C_{11} - 3C_{18})\sin 4\phi \cos\theta_m. \quad (51)$$

The total effective coupling C_{eff} is then

$$C_{\text{eff}} = \frac{2\pi}{\lambda_{2\omega_0}}\frac{d_3 d_5}{n_4 \Delta k_5} + C_2. \quad (52)$$

For this configuration, $\theta_m = 61.3°$, $\phi = \pi/4$, $\Delta k_5 = k_{3\omega}^e - k_{2\omega}^e - k_\omega^o = 1906\,\text{cm}^{-1}$, $n_4 = n_{2\omega}^e = 1.4771$, $d_3 = -0.315$ pm/V, and $d_5 = 0.285$ pm/V.

The value for C_{eff} measured was approximately $6 \pm 2 \times 10^{-24}\,\text{m}^2/\text{V}^2$. This is much smaller than that reported in Ref. 51 but is larger than the $8 \times 10^{-25}\,\text{m}^2/\text{V}^2$ given in Ref. 12. Again, inserting the various values into Eq. (52) gives either $C_2 = 2$ or $10 \times 10^{-24}\,\text{m}^2/\text{V}^2$, depending on the relative signs of the second-order and third-order contributions. The resulting value for $C_{11} - 3C_{18}$ is then 1.8 or $9 \times 10^{-23}\,\text{m}^2/\text{V}^2$, which is again larger than the $0.7 \times 10^{-24}\,\text{m}^2/\text{V}^2$ reported by Akhmanov *et al.*[12] Because of the very small value for C_{eff}, the efficiency of THG in KD*P is much less, 0.005% at 50 GW/cm^2. Scaling to the intensities used for BBO and d-LAP would give 0.08% at 200 GW/cm^2. Finally, it can be observed from Eqs. (48)–(51) that both the second- and third-order parts of C_{eff} have a $\sin 4\phi$ dependence on the azimuthal angle, and so there is no way to resolve C_{eff} into its component parts. In any event, it is clear that KD*P is not an effective material for single-crystal THG.

6. CONCLUSION

Cascaded second-harmonic generation and sum-frequency generation, even though nonphase matched, can contribute significantly, and even play the dominant role, in phase-matched single-crystal THG in materials with a second-order response. Up to 6% of the incident light has been converted to the UV in a single crystal of BBO for either type I or type II phase matching. Other materials, either those with large values of $\chi^{(3)}$ or with large $\chi^{(2)}$ elements not normally phase matchable, may prove to be even more effective.

The fact that the cascaded second-order coupling has a different azimuthal dependence than the third-order nonlinearity was used to obtain values for tensor elements of $\chi^{(3)}$ of BBO: $C_{10} = 1.8 \times 10^{-23}\,\text{m}^2/\text{V}^2$ and $0.15C_{11} + 0.54C_{16} = 4.0 \times 10^{-23}\,\text{m}^2/\text{V}^2$, dependent solely on the accuracy of the values used for d_{ij}. LAP can also reach conversion efficiencies in the 1% range, and further exploration of its parameter space is probably worthwhile. KD*P, however, was found to be an unsuitable material for single-crystal THG because of the relatively small values for the second- and third-order susceptibilities. In principle, single-crystal third-harmonic conversion efficiencies of 30%–40% are theoretically possible for drive irradiances >500 GW/cm^2. Femtosecond pulses enable achieving these high irradiances while remaining below the damage threshold of the material. However, the observation of gray tracking in BBO indicates that the damage mechanisms in the ultraviolet must also be considered.

ACKNOWLEDGMENTS

This work was performed under the auspices of the U.S. Department of Energy by Lawrence Livermore National Laboratory under contract W-7405-ENG-48.

*Current address: General Atomics, P.O. Box 85608, San Diego, California 92186-5608.

REFERENCES

1. J. F. Ward and G. H. C. New, "Optical third harmonic generation in gases by a focused laser beam," Phys. Rev. **185**, 57–72 (1969).
2. R. B. Miles and S. E. Harris, "Optical third-harmonic gen-

eration in alkali metal vapors," IEEE J. Quantum Electron. **QE-9**, 470–484 (1973).
3. J. C. Diels and F. P. Schafer, "Phase-matched third-harmonic generation in dye solutions," Appl. Phys. **5**, 197–202 (1974).
4. C. G. Durfee III, S. Backus, H. C. Kapteyn, and M. M. Murnane, "Intense 8-fs generation in the deep ultraviolet," Opt. Lett. **24**, 697–699 (1999).
5. B. C. Stuart, M. D. Feit, S. Herman, A. M. Rubenchik, B. W. Shore, and M. D. Perry, "Nanosecond-to-femtosecond laser-induced breakdown in dielectrics," Phys. Rev. B **53**, 1749–1761 (1996).
6. D. Strickland and G. Mourou, "Compression of amplified chirped optical pulses," Opt. Commun. **56**, 219–221 (1985).
7. M. D. Perry and G. Mourou, "Terawatt to petawatt subpicosecond lasers," Science **264**, 917–924 (1994).
8. P. Qiu and A. Penzkofer, "Picosecond third-harmonic light generation in β-BaB_2O_4," Appl. Phys. B **45**, 225–236 (1988).
9. I. V. Tomov, B. Van Wonterghem, and P. M. Rentzepis, "Third-harmonic generation in barium borate," Appl. Opt. **31**, 4172–4174 (1992).
10. C. Flytzanis and N. Bloembergen, "Infrared dispersion of third-order susceptibilities in dielectrics: retardation effects," Prog. Quantum Electron. **4**, 271–300 (1976).
11. G. R. Meredith, "Lower order effects in nonlinear two- and three-photon resonance spectroscopies," J. Chem. Phys. **75**, 4317–4325 (1981).
12. S. A. Akhmanov, L. B. Meisner, S. T. Parinov, S. M. Saltiel, and V. G. Tunkin, "Cubic nonlinear susceptibilities of crystals in the optical band; the signs and magnitudes of the susceptibilities of crystals with and without centers of inversion," Sov. Phys. JETP **46**, 898–907 (1977).
13. V. V. Rostovtseva, A. P. Sukhorukov, V. G. Tunkin, and S. M. Saltiel, "Higher harmonics generation by cascade processes in focused beams," Opt. Commun. **22**, 56–60 (1977).
14. X. Mu, M. V. Makarov, and Y. J. Ding, "Generation of blue light in Ce:$KTiOPO_4$ crystals using subpicosecond laser pulses," presented at the 1999 OSA Annual Meeting, Santa Clara, Calif., September 26–30, 1999.
15. M. S. Webb, D. Eimerl, and S. P. Velsko, "Wavelength insensitive phase-matched second-harmonic generation in partially deuterated KDP," J. Opt. Soc. Am. B **9**, 1118–1127 (1992).
16. P. N. Butcher and D. Cotter, *The Elements of Nonlinear Optics*, Cambridge Studies in Modern Optics (Cambridge University, Cambridge, UK, 1990).
17. C. Flytzanis, in *Quantum Electronics*, H. Rabin and C. L. Tang, eds. (Academic, New York, 1975), Vol. I, Part A, Chap. 2.
18. G. R. Meredith, "Cascading in optical third-harmonic generation by crystalline quartz," Phys. Rev. B **24**, 5522–5532 (1981).
19. G. R. Meredith, "Second-order cascading in third-order nonlinear optical processes," J. Chem. Phys. **77**, 5863–5871 (1982).
20. P. S. Banks, M. D. Feit, and M. D. Perry, "High-intensity third-harmonic generation in beta berium borate through second-order and third-order susceptibilities," Opt. Lett. **24**, 4–6 (1999).
21. D. A. Roberts, "Simplified characterization of uniaxial and biaxial nonlinear optical crystals: a plea for standardization of nomenclature and conventions," IEEE J. Quantum Electron. **28**, 2057–2074 (1992).
22. "Standards on piezoelectric crystals," Proc. IRE **37**, 1378–1395 (1949).
23. "IEEE standards on piezoelectricity," IEEE/ANSI Std. 176–1987 (Institute of Electrical and Electronics Engineers, New York, 1987).
24. P. N. Butcher, "Nonlinear optical phenomena," Tech. Rep. Bull. 200, Eng. Exp. Station (Ohio State University, Columbus, Ohio, 1965).
25. Y. Zhao, "The spatial symmetry of the third-order susceptibility tensor," IEEE J. Quantum Electron. **QE-22**, 1012 (1986).
26. C. C. Shang and H. Hsu, "The spatial symmetric forms of third-order nonlinear susceptibility," IEEE J. Quantum Electron. **QE-23**, 177–179 (1987).
27. R. W. Boyd, *Nonlinear Optics* (Academic, San Diego, Calif., 1992).
28. S. Singh, in *CRC Handbook of Laser Science and Technology*, M. J. Weber, ed., (CRC Press, Boca Raton, Fla., 1986), Vol. III, Part 1.
29. X. Yang and S. Xie, "Expression of third-order effective nonlinear susceptibility for third-harmonic generation in crystals," Appl. Opt. **34**, 6130–6135 (1995).
30. J. E. Midwinter and J. Warner, "The effects of phase matching method and of crystal symmetry on the polar dependence of third-order non-linear optical polarization," Brit. J. Appl. Phys. **16**, 1667–1674 (1965).
31. Y. X. Fan, R. C. Eckardt, R. L. Byer, C. Chen, and A. D. Jiang, "Barium borate optical parametric oscillator," IEEE J. Quantum Electron. **25**, 1196–1199 (1989).
32. R. C. Eckardt, H. Masuda, Y. X. Fan, and R. L. Byer, "Absolute and relative nonlinear optical coefficients of KDP, KD*P, BaB_2O_4, $LiIO_3$, MgO:$LiNbO_3$, and KTP measured by phase-matched second-harmonic generation," IEEE J. Quantum Electron. **26**, 922–933 (1990).
33. D. Eimerl, L. Davis, S. Velsko, E. K. Graham, and A. Zalkin, "Optical, mechanical, and thermal properties of barium borate," J. Appl. Phys. **62**, 1968–1983 (1987).
34. I. Shoji, H. Nakamura, K. Ohdaira, T. Kondo, R. Ito, T. Okamoto, K. Tatsuki, and S. Kubota, "Absolute measurement of second-order nonlinear-optical coefficients of β-BaB_2O_4 for visible to ultraviolet second-harmonic wavelengths," J. Opt. Soc. Am. B **16**, 620–624 (1999).
35. D. H. Jundt, Crystal Technology, Palo Alto, Calif. 94303 (personal communication, 1996).
36. M. D. Feit and J. A. Fleck, Jr., "Computation of mode properties in optical fiber waveguides by a propagating beam method," Appl. Opt. **19**, 1154–1164 (1980).
37. G. P. Agrawal, *Nonlinear Fiber Optics* (Academic, San Diego, Calif., 1989).
38. J. M. Burzler, S. Hughes, and B. S. Wherrett, "Split-step Fourier methods applied to model nonlinear refractive effects in optically thick media," Appl. Phys. B **62**, 389–397 (1996).
39. R. E. Bridges, R. W. Boyd, and G. P. Agrawal, "Multidimensional coupling owing to optical nonlinearities. I. General formulation," J. Opt. Soc. Am. B **13**, 553–559, 560–569 (1996).
40. J. A. Fleck Jr., J. R. Morris, and M. D. Feit, "Time-dependent propagation of high energy laser beams through the atmosphere," Appl. Phys. B **10**, 129–160 (1976).
41. F. Hache, A. Zeboulon, G. Gallot, and G. M. Gale, "Cascaded second-order effects in the femtosecond regime in β-barium borate: self-compression in a visible femtosecond optical parametric oscillator," Opt. Lett. **20**, 1556–1558 (1995).
42. C. Greninger, J. Marburger, and D. R. White, "Influence of third-order nonlinearity on second-harmonic generation," IEEE J. Quantum Electron. **QE-8**, 543–544 (1972).
43. T. Ditmire, A. M. Rubenchik, D. Eimerl, and M. D. Perry, "Effects of cubic nonlinearity on frequency doubling of high-power laser pulses," J. Opt. Soc. Am. B **13**, 649–655 (1996).
44. C. Y. Chien, G. Korn, J. S. Coe, J. Squier, G. Mourou, and R. S. Craxton, "Highly efficient second-harmonic generation of ultraintense Nd:glass laser pulses," Opt. Lett. **20**, 353–355 (1995).
45. C. Schwan, A. Penzkofer, N. J. Marx, and K. H. Drexhage, "Phase-matched third-harmonic generation of Nd: glass-laser picosecond pulses in a new cyanine-dye solution," Appl. Phys. B **57**, 203–211 (1993).
46. A. J. Taylor, G. Rodriguez, and T. S. Clement, "Determination of n_2 by direct measurement of the optical phase," Opt. Lett. **21**, 1812–1814 (1996).
47. R. DeSalvo, D. J. Hagan, M. Sheik-Bahae, G. Stegeman, and E. W. Van Stryland, "Self-focusing and self-defocusing by cascaded second-order effects in KTP," Opt. Lett. **17**, 28–30 (1992).
48. R. Danielus, P. Di Trapani, A. Dubietis, A. Piskarskas, D. Podenas, and G. P. Banfi, "Self-diffraction through cascaded

second-order frequency-mixing effects in β-barium borate," Opt. Lett. **18**, 574–576 (1993).
49. G. I. Stegeman, D. J. Hagan, and L. Torner, "$\chi^{(2)}$ cascading phenomena and their applications to all-optical signal processing, mode-locking, pulse compression and solitons," Opt. Quantum Electron. **28**, 1691–1740 (1996).
50. D. Eimerl, S. Velsko, L. Davis, F. Wang, G. Loiacono, and G. Kennedy, "Deuterated L-arginine phosphate: a new efficient nonlinear crystal," IEEE J. Quantum Electron. **25**, 179–193 (1989).
51. M. Okada, "Third-order nonlinear optical coefficients of $LiIO_3$," Appl. Phys. Lett. **18**, 451–452 (1971).